Ketamine restores escape behavior by re-engaging dopamine systems to drive cortical spinogenesis

Wu, M, Minkowicz, S, Dumrongprechachan, V, Hamilton, P, Xiao, L, Kozorovitskiy, Y*

Department of Neurobiology, Northwestern University, Evanston, IL 60208

*Corresponding author: Yevgenia.Kozorovitskiy@northwestern.edu

Abstract:

Escaping aversive stimuli is essential for complex organisms, but prolonged exposure to stress leads to maladaptive learning. Stress alters neuronal activity in distributed networks, plasticity, and neuromodulatory signaling; yet, the field lacks a unifying framework for its variegated sequelae. Here we build this framework using learned helplessness paradigm, where ketamine restores escape behavior after aversive learning. Low-dimensional optical readout of dopamine (DA) neuron activity across learning predicts acute behavioral responses, transitions through learning phases, and future sensitivity to ketamine treatment. Ketamine's effects are blocked by chemogenetic inhibition of DA signaling and mimicked by optogenetic activation. We use 2-photon glutamate uncaging/imaging to interrogate structural plasticity in medial prefrontal cortex, revealing that dendritic spinogenesis on pyramidal neurons is regulated by aversive experience and recovered by ketamine in a DA-dependent manner. Together, these data describe recurrent circuits that causally link neuromodulatory dynamics, aversive learning, and plasticity enhancements driven by a therapeutically promising anti-depressant.

Ketamine and its S-enantiomer esketamine, which act as antagonists of the glutamatergic N-methyl-D-aspartate (NMDA) receptors, demonstrate rapid onset anti-depressant effects in clinical trials[1,2]. Previous studies have shown that ketamine ameliorates depressive-like behaviors in animal models following acute or prolonged stress[3–7]. Accumulating evidence implicates the enhancement of synaptic plasticity in ketamine's behavioral effects[5,6,8–12]. However, which neural circuit dynamics mediate the effects of this rapidly acting antidepressant on behavior and plasticity are currently unknown.

Changes in reward-based and aversive learning represent features of depressive disorders that can be modeled in rodents[13–15]. One established model of aversive learning is learned helplessness[16–18]. Following prolonged inescapable stress exposure, animals learn that outcomes are independent of their behavioral actions; this learning eventually diminishes attempts to escape from avoidable stressful stimuli[19]. Specific activity patterns of dopaminergic (DA) neurons in the ventral tegmental area (VTA), and downstream DA release, encode reward and aversion[20–24]. This activity is differentially modulated by acute and chronic stress[25–27], regulating depressive-like behaviors[28–30]. A recently published meta-analysis suggests that acute sub-anesthetic doses of ketamine may increase DA levels in the cortex, dorsal striatum, and nucleus accumbens[31,32], but the causal relationship between the DA system and ketamine's effects on neural plasticity and behavior remains to be elucidated.

Low dimensional readout of DA neuron activity dynamics in aversive learning

To define the function of midbrain DA neurons during aversive learning, we used a modified model of learned helplessness[5,32]. Briefly, a shuttle box containing two regions connected by a door allows animals to escape from one side to the other when an electric foot shock is delivered to either side. Naive mice avoid *escapable* aversive stimuli. However, following repeated exposure to *inescapable* foot shocks, subjects reduce escapes from readily avoidable aversive stimuli (Figure 1a, b). Our data and prior publications[32] suggest that a single low dose of racemic ketamine (10 mg/kg, b.w., i.p.) is sufficient to rescue escape behavior in this aversive learning paradigm (Figure 1b). We then used fiber photometry to obtain a low dimensional optical readout of population activity of VTA DA neurons, expressing genetically encoded calcium indicator GCaMP6f. DAT^{icre} neonates were virally transduced with Cre-dependent AAV1.CAG.Flex.GCaMP6f. Four to six weeks after transduction, optical fibers were implanted in the VTA (Figure 1c), guided by real-time photometry readout (Extended Data Figure 1a). The activity of VTA DA neurons was evaluated during aversive learning in P40-60 mice of both sexes, with Ca^{2+} transient shape varying across the phases of learning. Surgical anesthesia during fiber implant procedure was associated with ~1 Hz oscillations in VTA calcium transients (Extended Data Figure 1b).

At the start of learning (Baseline), the activity of VTA DA neurons first decreases during the aversive foot shocks, rising after the termination of the shock (Figure 1d, e; Extended Data Figure 1c, d). This biphasic response is consistent with recently published observations of VTA DA activity during other forms of aversive conditioning[34]. After two days of induction (learned helplessness, LH), the responses of VTA DA neurons to foot shocks are profoundly blunted. In parallel to the behavioral rescue, a single low dose of racemic ketamine (10 mg/kg, b.w., i.p., LH+KET) largely restored characteristic Ca^{2+} transient features (Figure 1d, e). Visualizing sequential Ca^{2+} traces from a single animal illustrates (1) the prevalence of post-stimulus peaks at the start of learning, (2) their decreased latency relative to shock onset during the second day of training, and (3) the recovery of Ca^{2+} transient latency to peak following ketamine administration (Figure 1f). To quantify this temporal structure, we computed the latency to peak on averaged trials for every animal (n = 10 trials/avg) and plotted the data across days of learning as a scatter plot and cumulative distribution (Figure 1g).

Since the activity of DA neurons has been linked to movement[35,36], one potential explanation for how aversive learning could modulate Ca^{2+} activity of VTA DA neurons is by altering locomotor behavior. However, we

observed no differences in open field locomotion across phases of learning (Figure 1h). Changes in VTA DA neuron activity were not associated with motion transitions (Figure 1i and Extended Data Figure 1e). These experiments demonstrate that VTA DA neuron activity is restructured by aversive learning. The native structure of DA transients is recovered by ketamine in parallel to escape actions, independently of gross motor changes.

To better understand the relationship between VTA DA neuron activity and single trial behavioral responses, we leveraged the analog tunability of LH to design a graded learning paradigm (gLH) with only a single induction day and a large number of escapable foot shocks as the test stimuli (Figure 2a and Extended Data Figure 2a). As anticipated, a more gradual emergence of learning is observed in this paradigm compared to stronger LH (sLH, 2 induction days, Figure 1), which again recovered with ketamine (Figure 2b). A three-state transition model depicts the probability of transitioning between behavioral responses, allowing us to compare patterns of response sequences across learning (Figure 2c).Quantifying the similarity of behavioral sequencing across the phases of learning as one minus the Frobenius norm of the difference between model pairs ($1 - norm(model_a - model_b)$), the similarity between baseline and gLH models is 0.64, between baseline and gLH + KET it is 0.73, and 0.65 between gLH and gLH + KET. A response is labeled premature if the animal spontaneously runs to the other side of the chamber during the random length pretrial time. Baseline and post ketamine sequences of behavioral responses are more similar to each other than either is to gLH.

The gradual emergence of learning in gLH enabled broad sampling of Ca^{2+} transients for outcome-specific response trials. Separately plotting VTA DA neuron activity for trials where the animal escaped or failed to escape reveals that each behavioral response is associated with distinct Ca^{2+} transient shapes (Figure 2d). Escape trial transients are monophasic, with an increase in fluorescence following the end of stimulus and successful transition to the other side of the box. In contrast, biphasic transients, where fluorescence decreases during the stimulus and increases afterwards, accompany failures to escape. The negative transients prevalent during failure trials in gLH are reminiscent of the negative deflections in sLH, observed in the baseline condition, blunted after aversive learning, and re-emerging following ketamine treatment (Figure 1d). In contrast to the dampening of VTA DA signal seen after aversive learning with the strong induction paradigm, graded learning is associated with no overall loss of the response, but instead an increase in the similarity of the activity patterns between escape and failure trials (Figure 2e). Latencies to both positive and negative peaks in Ca^{2+} transients vary between escape and failure trials, and these latency differences were relatively smaller during gLH (Extended Data Figure 2b). We also noted a modest increase in overall fluorescence level arising after termination of behavioral testing that emerged during learning (Extended Data Figure 2c).

In humans and other animals, individual variability in stress susceptibility and responsiveness to neuroactive compounds is broadly acknowledged[37]. To track individual evolution of behavior, learning curves were constructed by starting at 0 and incrementing by 1 for every escape trial, decrementing by 1 for every failure, and keeping constant for spontaneous, or premature, transitions (Figure 2f).In contrast to the relatively similar behavioral trajectories during baseline and gLH, dramatic individual differences emerge after ketamine treatment. To depict the relationship between an animal's ketamine responsiveness and VTA DA activity, we plot the Euclidean norm of the difference between their Ca^{2+} transients during escape and failure trials ($||escape - failure||_2$) across learning (Figure 2g). We can fit a line to the cumulative response graph (Figure 2f) for each individual in every behavioral phase to generate its slope – a single number that captures the animal's behavioral response dynamics. Figure 2h shows a positive correlation between behavioral response to ketamine (response slope) and the change in the similarity between Ca^{2+} transients during escape and failure trials after ketamine treatment (trace distance slope). Stronger ketamine behavioral effects are linked

to more distinct Ca^{2+} transients between escape and failure trials (R^2 = 0.720). Intriguingly, individuals with large differences between DA calcium signals on escape and failure trials in the baseline condition respond more strongly to future ketamine treatment (Figure 2i, R^2 = 0.704). Thus, individual response to ketamine can be predicted from this difference in VTA DA neuron activity during baseline (Figure 2i), well before any behavioral differences between animals emerge (Figure 2j, R^2 = 0.06).

DA neuron activity is necessary for behavioral effects of ketamine

The strong association between DA transients, behavioral states, and single trial responses raises the possibility that particular signatures of DA signals in response to aversive stimuli are required for escape actions. If so, the behavioral effects of ketamine in recovering escape actions and normalizing VTA DA transients should be abolished by inhibiting DA neuron activity. We tested this hypothesis by conditionally expressing an inhibitory DREADD (designer receptor exclusively activated by designer drug) hM4Di in VTA DA neurons. This engineered muscarinic receptor is activated by clozapine-N-oxide (CNO) to drive $G\alpha_i$-coupled pathways[38–41]. We used a chicken beta actin (CBA) promoter driven Cre-conditional hM4Di AAV, with expression in VTA DA neurons confirmed by immunofluorescence (Figure 3a). Electrophysiological efficacy was evaluated using cell-attached recordings of hM4Di-mCherry$^+$ VTA DA neurons, with a flow in and a washout of 1 µM CNO (Figure 3b).

Mice conditionally expressing hM4Di in VTA neurons were compared to their Cre$^-$ littermate controls in the strong LH paradigm. Here, two ketamine treatments were administered on sequential days – the first one with CNO, and the second one alone (Figure 3c). The expression of hM4Di in DA neurons did not change baseline behavior or learned helplessness induction. However, inhibiting DA neurons by CNO application (3 mg/kg, b.w., i.p.) co-administered with ketamine (10 mg/kg, b.w., i.p.) blocked ketamine's rescue of escape behaviors. This effect was evident 4 hrs after CNO/Ketamine treatment and persisted for 24 hrs. Yet, when ketamine was administered alone on the following day, the behavioral rescue in hM4Di$^+$ mice was recovered. Persistent LH was evident in multiple animals of both groups 72 hrs following the ketamine only treatment. Comparing behavioral responses to ketamine alone versus ketamine plus CNO within animals, at two separate time-points, shows that hM4Di$^-$ animals cluster around the unity line. In contrast, hM4Di$^+$ mice responses cluster above unity line, reflecting selective efficacy of ketamine treatment in the absence of CNO (Figure 3d).

The administration of CNO in a separate group of hM4di$^+$ mice in the baseline condition did not alter the proportion of failures to escape suggesting that decreasing the activity of VTA DA neurons has no effect on escape behavior prior to learning (Figure 3e). Also, locomotor behavior in the same animals was not grossly altered by a single CNO administration (-0.8048 ± 0.4486 m/min, Mean ± SEM of difference, paired t-test, p = 0.369). Altogether, these data support the necessity of VTA DA signaling in the behavioral reversal of aversive learning by ketamine, rather than in the native escape response in naïve animals.

Aversive experience and ketamine regulate mPFC DA activity and release

The activity of DA terminals in mPFC is involved in the processing of emotionally valenced information, including aversive stimuli[20,26,42]. In particular, the mPFC is linked to behavioral flexibility in humans and other animals[43,44]. The dopamine release in mPFC modulates its activity and plasticity[45], which is altered in animal models of stress[8,28]. To directly evaluate DA signaling in mPFC, we transduced neonatal mice with AAV1.CAG.Flex.GCaMP6f in the VTA, followed by unilateral fiber implants in the mPFC, and trained them in the sLH paradigm (Extended Data Figure 3a, b). Axonal signals could be detected in response to stimuli administration. The axonal signals were smaller than somatic signals examined previously, but followed the same general structure (Extended Data Figure 3c, d). Next, in order to more specifically sense dopamine release, rather than axonal Ca^{2+} influx, we turned to a recently developed genetically encoded DA sensor

dLight1.1[46]. We created a Cre-dependent AAV expressing dLight1.1 under the control of the CBA promoter. This specificity was important, because different DA receptors are expressed in distinct subsets of mPFC neurons[47–49]. We evaluated dLight1.1 reported DA signals in Drd1$^+$ neurons of mPFC. Drd1-Cre-FK150 mice (~P30) of both sexes that were virally transduced with AAV1.CBA.DIO.dLight1.1 in mPFC and implanted with optical fibers (Extended Data Figure 3e, f). We found robust DA transients in mPFC Drd1a$^+$ neurons in response to foot-shock, which were blunted after sLH, and recovered with ketamine administration along with escape behavior (Extended Data Figure 3g, h). The timing of positive deflection peaks for dLight preceded that of VTA DA somatic or axonal calcium transients (Extended Data Figure 3h). One potential explanation for this observation is that functionally significant amounts of DA could release from local axons prior to sufficient accumulation of calcium required for GCaMP6f readout. Altogether, our data suggest that dopamine signaling in mPFC, like somatic and axonal Ca^{2+} photometry, carries a signature of the animal's behavioral state.

Evoked plasticity in mPFC is regulated by aversive experiences in a dopamine-dependent manner

Ketamine is widely believed to generate its therapeutic effects, at least in part, by modulating plasticity of mPFC neurons[4,5,10,11 50]. Several prior studies demonstrate that *in vivo* administration of ketamine enhances dendritic spine density[8,51–53] and restores dendritic spine loss[12]. Whether ketamine directly increases spinogenesis and synaptogenesis, or alternatively, decreases neuronal synapse maintenance and turnover, remains unclear. To answer this question and to evaluate whether changes in DA signaling contribute to ketamine regulation of mPFC plasticity, we turned to focal induction of *de novo* spinogenesis using 2-photon uncaging of glutamate.

Acute slices of mPFC were prepared from P25-40 mice of both sexes, following neonatal transduction of sparse EGFP expression, accomplished by a combination of AAV1.hSyn.Cre and AAV8.DIO.EGFP. We imaged EGFP-labeled dendrites of layer 5 pyramidal neurons in mPFC using 2-photon laser scanning microscopy (2PLSM, 910 nm). A second laser was tuned to 725 nm to locally uncage MNI-glutamate near dendrites to induce new dendritic spines (Figure 4a), as previously described for developing neurons in the striatum and superficial layers of sensory and motor cortex[41,54,55]. This evoked spinogenesis assay was carried out in control animals with or without ketamine treatment. Separately, we evaluated glutamate evoked spinogenesis in mice during different stages of aversive learning (baseline, LH, and LH+KET), in the presence or absence of additional acute stress (Figure 4b), since prior studies of experience-induced structural changes in the brain report distinct and sometimes opposite effects of acute and chronic stress[9]. Successful and unsuccessful induction trials of *de novo* spinogenesis were clearly distinguished by z-stack projections through a dendritic segment prior to and following the brief induction protocol (< 30 sec) of up to 40 uncaging pulses (Figure 4c and Extended Data Figure 4a). A single *in vivo* administration of ketamine in naïve animals enhanced evoked *de novo* spinogenesis two hours after treatment, compared to saline-treated controls (Figure 4d). These data suggest that ketamine – in the absence of aversive learning – is capable of directly enhancing glutamate-dependent spinogenesis, elucidating the mechanism that explains prior reports of dendritic spine density differences associated with ketamine treatment.

Next we examined glutamate evoked *de novo* spinogenesis on mPFC neurons from mice across distinct behavioral states. Acute stress exposure (90 foot shocks, 3 sec, 0.3 mA, randomized timing) in the baseline condition significantly enhanced evoked *de novo* spinigenesis on pyramidal neurons in mPFC. Following aversive learning, the probability of spinogenesis was decreased compared to baseline, and the plasticity-promoting effect of acute stress was abolished. In separate groups of animals, ketamine rescued this potentiation of evoked plasticity by acute stress, as well as increased spinogenesis overall (Figure 4e). These

effects were similar in males and females, as depicted in the binary grid plots of individual induction trials (Figure 4f).

To determine whether ketamine's effect on evoked plasticity is mediated by the activation of dopamine receptors, we first verified the expression of Drd1a receptors in GFP-expressing neurons. Consistent with prior reports[56], the majority of pyramidal neurons in the deep layers of mPFC express *Drd1a* mRNA (Figure 4g).Similar distributions of Drd1a-expressing mPFC neurons are observed in Drd1-Cre-FK150; tdTomato cross (Extended Data Figure 4b). We compared glutamate-evoked spinogenesis after administering ketamine alone, or in conjunction with a Drd1 receptor antagonist SKF83566 (10 mg/kg i.p., 2 hrs prior to *ex vivo* experiments). We found that the Drd1 antagonist blocked ketamine's potentiation of spinogenesis, while the antagonist treatment alone had no effect (Figure 4h). Although the activation of Drd1 receptors in this neuronal population is not required for baseline glutamate-evoked plasticity, it appears to be necessary for ketamine's enhancement of evoked spinogenesis. As a complement to pharmacological manipulation of Drd1 receptors, since SKF83566 treatment *in vivo* broadly alters Drd1 activation and movement, we turned again to chemogenetic inhibition of VTA DA neurons to modulate downstream DA release. Inhibiting hM4Di^{+} VTA DA neurons with CNO (3 mg/kg, i.p.) blocked spinogenesis enhancing effects of either ketamine or acute stress exposure (Figure 4i). Yet, for baseline Drd1 blockade, we observed no effects of CNO treatment in the absence of another manipulation that alters plasticity. Altogether, our data show that Drd1 activation controls mPFC metaplasticity, mediating the effects of acute and prolonged stress, as well as the actions of ketamine.

Closed loop interactions between VTA and mPFC in aversive learning

If the impairment of escape behavior after aversive learning is caused by blunted DA release in mPFC, increasing local dopamine release after learned helplessness should rescue escapes. To test this prediction, we optogenetically activated DA terminals in mPFC in animals with ChR2 expression restricted to VTA DA neurons. DAT^{icre} neonates were transduced with AAV1.EF1α.DIO.hChR2(H134R).eYFP and implanted with optical fibers (~P40) four to six weeks after transduction (Figure 5a, b). Following learned helplessness induction, during the test session animals received a series of burst optogenetic stimuli at 20 Hz every 10 sec (10 pulses, 20 ms width, 500 ms duration), instead of ketamine (Figure 5c). Note that the stimulation bursts were not timed relative to shocks. Optogenetic activation of DA axon terminals in mPFC significantly decreased the percentage of failures after LH, as well as latencies to escape (Figure 5d). Again, locomotion behavior did not change during optogenetic stimulation (Figure 5e).Thus, enhancing DA release in mPFC is sufficient to rescue escape behavior after aversive learning.

While we find that systematically inhibiting VTA DA neuron activity abolishes the behavioral effect of ketamine and mPFC plasticity changes, whether the behavioral response to ketamine primarily operates through local dopamine release in mPFC remains unclear. To achieve local inhibition of dopamine release, we infused CNO into mPFC of mice expressing hM4Di in VTA DA neurons and their terminal in mPFC, to reduce axonal release probability[38,57,58]. DAT^{iCre} neonates were transduced with AAV1.CBA.DIO.hM4Di.mCherry in the VTA, and cannulae were implanted bilaterally over mPFC (at ~P50) in order to locally deliver 1 mM CNO (1 µl for each side) (Figure 5f and Extended Data Figure 5a). A high density of hM4Di mCherry expression in mPFC terminals was observed in immunoehnanced fixed tissue sections (Figure 5g). Local infusion of CNO in mPFC blocked the behavioral effect of ketamine in the aversive learning paradigm, while ketamine alone was sufficient to rescue escape behavior the following day (Figure 5h and Extended Data Figure 5b). These data are consistent with our prior experiments on the inhibition of VTA DA neurons (Figure 3, i.p. injection of CNO), but the sufficiency of an mPFC-specific activation of hM4Di suggests that mPFC is the key site of control over behavioral changes driven by ketamine.

The activation of Drd1 receptors initiates $G\alpha_s$-cAMP-PKA signaling cascades, which enhance spinogenesis, synaptic transmission, and neuronal activity[40,41,56,59]. We therefore used chemogenetics to selectively activate Drd1 expressing neurons in mPFC using a $G\alpha_q$-coupled hM3D by expressing AAV2.hSyn.DIO.hM3Dq.mCherry in Drd1-cre-FK150 mice during aversive learning. The expression and functional activation of hM3Dq expressed on Drd1$^+$ mPFC pyramidal neurons were verified by immunohistochemistry and electrophysiology (Figure 5i, j). The expression of hM3Dq alone did not change baseline escape and failure rates or the magnitude of aversive learning. After LH induction, a single dose of CNO was sufficient to rescue escape behavior within 2 hours, with a larger effect observed after 4 hours (Figure 5k). Activating Drd1a-expressing neurons in mPFC did not change total distance traveled over a 10 minute period (Figure 5l), suggesting that the recovery of escape behavior is not due to an overall enhancement of locomotion. At the end of the experiment, the enhancement of neuronal activity was further validated by observing increased c-fos expression in mCherry$^+$ neurons (Figure 5m).In addition to these results, a recently published study showed that optogenetic activation of Drd1$^+$ mPFC neurons decreases immobility time in the forced swim test, suggesting the possibility that these Drd1-expressing neurons may regulate general aversive or active coping responses [60]. Altogether, our data demonstrate that activating DA-sensing mPFC neurons is sufficient to rescue escape behavior after aversive learning.

While mPFC receives dopaminergic input from the VTA, it also sends excitatory glutamatergic projections back to VTA DA neurons, based on trans-synaptic tracing analyses and optogenetic assays[42,61–63]. Whether this recurrent VTA-mPFC circuit reflects a closed-loop interaction, involving the same neurons in the VTA and Drd1$^+$ neurons in mPFC, is unclear. To label neurons that send projections to VTA, we injected red retrograde tracer fluorescent beads in the VTA (Extended Data Figure 6a, b). Combined retrograde tracing and FISH experiments demonstrate that the majority of retrobead$^+$ neurons in layer V of mPFC express *Drd1a* mRNA, suggesting they receive dopaminergic inputs. In contrast, a small fraction of the retrobead$^+$ neurons in layer 2/3 of mPFC have *Drd1a* mRNA (Extended Data Figure 6c).To determine whether mPFC projecting VTA neurons also receive mPFC projections, we expressed AAV8.DIO.GFP in Drd1-Cre-FK150 animals and injected retrobeads in mPFC (~P30) (Extended Data Figure 6d). Consistent with previous reports[63], most but not all mPFC-projecting VTA neurons express TH, indicating their dopaminergic identity (Extended Data Figure 6e).Anatomical tracing results show that mPFC-targeting VTA neurons reside in a region of dense projections from mPFC Drd1$^+$ neurons (Extended Data Figure 6f). Since glutamate co-transmission from VTA DA terminals has been reported in nucleus accumbens[64], next we recorded light-evoked, pharmacologically isolated, excitatory post-synaptic currents (EPSCs) in layer V mPFC pyramidal neurons of mice transduced with Cre-dependent ChR2 in the VTA (Extended Data Figure 6g). No time-locked or delayed light-evoked EPSCs were observed in the presence of a GABA(A) receptor antagonist (Extended Data Figure 6h), arguing for selective release of DA onto deep layer mPFC pyramidal neurons. Altogether, these data support the existence of a recurrent closed loop of VTA and mPFC neurons which amplifies DA signaling through glutamate and is modulated by ketamine (Extended Data Figure 6i).

Discussion

Animals must learn to avoid dangerous stimuli in nature in order to survive, underscoring the ethological significance of aversive learning. However, overlearned responses can be maladaptive. Prolonged exposure to stressful events can lead to learned helplessness[19,33,65], where an individual fails to avoid unpleasant stimuli. Here, we demonstrate that aversive learning restructures neuronal activity in the VTA DA system, causing a shift in behavioral outcome distribution. A single low dose ketamine treatment suffices to normalize both DA signaling and behavior, with the efficacy of treatment predicted by VTA DA activity features prior to learning. Moreover, bidirectional manipulations of distinct components of DA signaling occlude or mimic the effects of ketamine. Ketamine modulation of DA activity transforms mPFC synaptic structural plasticity and interacts

with experience-dependent plasticity dynamics, as evidenced by glutamate uncaging-evoked formation of new dendritic spines on deep layer pyramidal neurons. In our model, ketamine changes neural activity and plasticity within reciprocally connected VTA-mPFC circuits to rescue ethological meaningful escape behaviors after aversive learning.

Multivalenced encoding of information by VTA DA neurons and their projections is now well established[20,21,66–68]. In our framework, the differences in VTA DA activity between outcomes maps to the tendency to escape aversive stimuli. Accordingly, decreases in the differences between escape and failure trials after aversive learning, elicited by learning or by inhibiting VTA DA neuron activity, are associated with failing to escape avoidable stressful stimuli. Given the observations that DA neurons process information that translates into decisions for future actions[36,69–71], predictions of behavioral outcomes can be made based solely on DA neuron activity. Future behavioral responses to ketamine are predicted from escape/failure calcium photometry trace distances in the baseline condition, before learning occurs. In the three state behavior transition models with graded learning, the baseline and ketamine treated groups present with higher probability of sequential escapes and failure-escape transitions, whereas gLH mice have a higher probability of sequenced failures. These models, in combination with photometry data, suggest that immediate prior experience is weighed differently in a state-dependent manner.

Recent evidence from human brain imaging studies suggests that major depressive disorder is associated with reduced synaptic connections, which are likely linked to the observed differences in network functional connectivity[72]. The long-standing theory for how stressful experience alters mPFC dendritic spines and synapses is shaped as an inverse parabolic function. Structural plasticity is enhanced by acute stress, but impaired after prolonged or chronic aversive experiences[9]. In our results, acute stress enhances the probability of spinogenesis, while chronic stress dampens it, with ketamine recovering both the baseline spinogenesis capacity, as well as the modulation by acute stress. This ketamine modulation of the rules for plasticity – or metaplasticity – depends on DA signaling, as evidenced by the requirement for Drd1 availability (Figure 5h) and VTA DA neuron activity (Figure 5i). Ketamine acts within this framework by shaping the activity of VTA DA neurons and local DA release to mediate changes in spinogenesis that is required for long-lasting behavioral improvement.

Acknowledgements

The authors are grateful to Lindsey Butler for mouse colony management, Northwestern Biological Imaging Facility and Dr. Tiffany Schmidt for confocal microscope access. This work was supported by the Rita Allen Foundation Scholar Award, NINDS R01NS107539, Searle Scholar Award, the Beckman Young Investigator Award, William and Bernice E. Bumpus Young Innovator Award, NARSAD Young Investigator and P&S Fund Grant (all Y.K.). M.W was supported as an affiliate fellow of the NIH T32 AG20506 and V.D. is a predoctoral fellow of the American Heart Association.

Author Contributions

M.W. and Y.K. designed the study. M.W. carried out most experiments and analyses in the study. S.M. made major contributions to behavioral analyses, V.D. created new plasmids, viruses, and contributed to experimental analyses. P.H. and L.X contributed to morphological analyses and functional validation of DREADD tools. All authors participated in writing the manuscript.

Competing Interests

The authors declare no competing interests.

Methods

Mouse strains and genotyping. Animals were handled according to protocols approved by the Northwestern University Animal Care and Use Committee. Weanling and young adult male and female mice (postnatal days 21-80) were used in this study. Approximately equal numbers of males and females were used for every experiment. All mice were group-housed, with standard feeding, light-dark cycle, and enrichment procedures; littermates were randomly assigned to conditions. C57BL/6 mice used for breeding and backcrossing were acquired from Charles River (Wilmington, MA), and all other mouse lines were acquired from the Jackson Laboratory (Bell Harbor, ME) and bred in house.

B6.SJL-Slc6a3$^{tm1.1(cre)Bkmn}$/J mice, which express Cre recombinase under control of the dopamine transporter promoter, are referred to as DAT^{iCre} [73]; B6.FVB(Cg)-Tg(Drd1-cre)FK150Gsat/Mmucd mice, which express Cre recombinase under control of the dopamine Drd1a receptor promoter, are referred to as Drd1-Cre-FK150 [74]. For a subset of experiments, Cre positive mice were crossed to a floxed tdTomato reporter strain (Ai14, Jackson Lab, #007914). All transgenic animals were backcrossed to C57BL/6 for several generations. Heterozygous Cre^{+} mice were used in experiments. Genotyping primers are available on the Jackson Lab website.

Stereotactic injections and optic fiber implants

Conditional expression of target genes in Cre-containing neurons was achieved using recombinant adeno-associated viruses (AAVs) encoding a double-floxed inverted open reading frame (DIO) of target genes, as described previously[41]. For fiber photometry experiments, DAT^{iCre} mice were transduced with AAV1.CAG.Flex.GCaMP6f.WPRE-SV40 (1.33 x 10^{13} GC/ml) from the UPenn viral core (Philadelphia, PA, a gift from the Genetically Encoded Neuronal Indicator and Effector Project (GENIE) and Douglas Kim; Addgene viral prep #100835-AAV1)[75]. For chemogenetic experiments, Drd1-cre-FK150 mice were transduced with AAV2.hSyn.DIO.hM3Dq.mCherry (8.6 x 10^{12} GC/ml) from Addgene (Cambridge, MA, a gift from Dr. Bryan Roth; Addgene viral prep # 44361-AAV2)[76], DAT^{iCre} mice were transduced with a custom built AAV1.CBA.DIO.hM4Di.mCherry (1.28 x 10^{13} GC/ml, Vigene Biosciences, Rockville, MD, plasmid a gift from Dr. Bernardo Sabatini[77]). For glutamate uncaging-evoked spinogenesis experiments, AAV8.CAG.Flex.EGFP (3.1 x 10^{12} GC/ml, UNC vector core, Dr. Ed Boyden) was co-injected with AAV1.hSyn.Cre.WPRE.hGH (1 x 10^{10}, UPenn viral core, Dr. James M. Wilson, unpublished) to achieve sparse expression in mPFC pyramidal neurons of C57BL/6 mice. For *in vivo* optogenetics experiments, DAT^{iCre} mice were transduced with AAV1.EF1a.DIO.hChR2(H134R).mCherry (1.2 x 10^{13} GC/ml) or AAV1.EF1a.DIO.hChR2(H134R).eYFP (3.55 x 10^{13} GC/ml), acquired from Dr. Karl Deisseroth (Addgene viral prep #20297/20298-AAV1). For retrograde labeling, mice were intracranially injected with Red Retrobeads™ (Lumafluor Inc.). For neonatal AAV delivery, P3-6 mice were cryoanesthetized, received ketoprofen for analgesia, and were placed on a cooling pad. Virus was delivered at a rate of 100 nl/min for up to 150-200 nl using an UltraMicroPump (World Precision Instruments, Sarasota, FL). Medial prefrontal cortex (mPFC) was targeted in the neonates by directing the needle immediately posterior to the eyes, 0.3 mm from midline, and 1.8 mm ventral to skin surface. Ventral tegmental area (VTA) was targeted in the neonates by directing the needle approximately ±0.2 mm lateral from Lambda and 3.8 mm ventral to skin surface. Coordinates were slightly adjusted based on pup age and size. Following the procedure, pups were warmed on a heating pad and returned to home cages.

For adult intracranial AAV or retrobeads injections, P25-30 mice were anesthetized with isoflurane (3% for induction value, 1.5-2% for maintenance) or ketamine:xylazine (100:12.5 mg/kg b.w.), received ketoprofen for analgesia, and were placed on a small animal stereotax frame (David Kopf Instruments, Tujunga, CA). AAVs or retrobeads were delivered unilaterally through a pulled glass pipette at a rate of 100 nl/min using an

UltraMicroPump (World Precision Instruments, Sarasota, FL). Injection coordinates for VTA, 2.8 mm posterior to bregma, 0.4 mm lateral, and 4.3 - 4.5 mm below the pia; for mPFC, 2.0 mm anterior to bregma, 0.4 mm lateral, and 1.3 - 1.6 mm below the pia. Pipettes were held at the injection location for 15 min following AAV or retrobead release. Coordinates were slightly adjusted based on mouse age and size. Mice recovered for 7-9 days and > 14 days following retrobead and AAV injections, respectively.

For photometry fiber placement in the VTA or mPFC, P40-60 mice were implanted with a 400 µm diameter 0.48 NA single mode optical fiber (Doric lenses, Quebec City, QC, Canada) directly above the VTA at -2.8 mm (AP); +0.4 mm (ML); 4.3 - 4.5 mm (DV), mPFC +2.0 mm (AP); +0.4 mm (ML); 1.3 - 1.6 mm (DV). For optogenetics in the mPFC, custom-made optical fibers were used (2 mm stub length, 200 µm diameter, 0.5 NA, FP200ERT, Thorlabs). Coordinates for mPFC fiber placement were +2.0 mm (AP), +0.4 mm (ML), and 1.3 - 1.6 mm (DV). For bilateral cannulation in mPFC: +2.2 mm (AP); 1.2 mm (DV), with center to center distance of 0.8 mm. Dummy cannulae with projections of 0.2 mm over the guide cannulae (2.5 mm) were inserted after implantation. Internal cannulae with projections of 0.5 mm were used for liquid delivery. Behavioral experiments were conducted 7-12 days after implantation. Real-time photometry recording was performed during optical fiber implant above the VTA, for optimal targeting. When the fiber tip approached the VTA region, a continuous increase of fluorescence intensity was observed. The final position of implantation was determined by the cessation of further increases in fluorescence intensity.

Behavior assays

Aversive learning. The strong learned helplessness procedure consisted of two induction sessions (1 session per day; 360 inescapable foot shocks per session; 0.3 mA, 3 sec; random 1-15 sec intershock intervals). Active/Passive Avoidance Shuttle Boxes from MazeEngineers (Boston, MA) were used for the experiment. To assess the degree of aversive learning, test sessions (30 escapable foot shocks per session; 0.3 mA, 10 sec; random 5-30 sec intershock intervals) were conducted before induction, 24 hrs after the last induction session, and following pharmacological or optogenetic manipulations. The testing was performed in a shuttle box (18 × 18 × 20 cm) equipped with a grid floor and a door separating the two compartments. Escapes were scored when the animal shuttled between compartments during the stimulus presentation. Escape latency was measured as the time from the start of the shock to the escape. The stimulus automatically terminated when the animal shuttled to the other compartment. Failures were scored when the animal failed to escape before the stimulus end (10 sec). All behavioral assays were conducted during the active phase of the circadian cycle.

To evaluate the effect of ketamine on learned helplessness behavior, a single dose of ketamine (10 mg/kg b.w., i.p.) was given 48 hrs after the last induction session, and the test session performed 4 hrs later. For chemogenetic activation in mPFC, 48 hrs after the last induction session Clozapine N-oxide (CNO) was administered i.p., followed by test sessions 2 hrs and 4 hrs later. For chemogenetic inhibition in VTA, the first CNO dose (3 mg/kg, i.p.) was co-administered with ketamine 48 hrs after the last induction, followed by test sessions 4 and 24 hrs later. Then, immediately following the last test session, Ketamine was administered alone, followed by test sessions 4, 24, and 72 hrs later. For optogenetic activation of DA terminals in the mPFC, 48 hrs after the last induction session a test session was performed with optogenetic stimulation (bursts were not time-locked to behavior and consisted of ten 20 ms long pulses at 20 Hz, with 500 ms long burst duration and 10 sec inter-burst interval).

For the graded aversive learning procedure, six test sessions were performed (1 session per day; 100 escapable foot shocks per session; 0.3 mA, 3 sec; random 5-15 sec intershock intervals). A single induction session (360 inescapable footshocks; 0.3 mA, 3 sec; random 1-15 sec intershock intervals) was performed at the end of the 2nd day. A single dose of ketamine (10 mg/kg b.w., i.p.) was given 4 hrs before the 5th test

session. The final test session was performed 24 hrs after ketamine treatment. Age-matched controls were given six test sessions, in the absence of induction sessions or ketamine treatment.

Open field locomotion. To assess the locomotor activity, mice were placed in the center of a plastic chamber (48 cm × 48 cm × 40 cm) in a dimly lit room. Mice explored the arena for 15 min, with video (30 fps) and photometry recording performed during the final 10 min.

Local drug infusion

To inhibit hM4Di-expressing DA terminals by local CNO infusion in mPFC, we used internal cannulae (28 gauge, Plastics One, Roanoke, VA) with 0.5 mm long projection beyond the implanted guide-cannula, as described above. 1 mM CNO (1 µL per side) was administered over a 2 min long injection period using a 10 µl Hamilton syringe (Hamilton Company, Franklin, MA). Dummy cannula with 0.2 mm projection were inserted back after the delivery of CNO. The first infusion was performed immediately before ketamine injection, and the two subsequent infusions were performed 1.5 and 3 hrs after ketamine injection. Learned helpless behaviors were assessed 4 and 24 hrs after ketamine treatment.

Fiber photometry

A modified version of Scanimage software[78] was used for data acquisition. Signals were sampled at 1 kHz and downsampled to 250 Hz for analysis. Fluorescence signal was baseline adjusted in non-overlapping 100 sec windows as $(signal - median(signal)) \,/\, median(signal)$, denoted as dF/F. Recordings were made during a subset of the sessions of learned helplessness and open field locomotion, as noted in the text.

Acute slice preparation and electrophysiology

Coronal brain slice preparation was modified from previously published procedures[40,41,79]. Animals were deeply anesthetized by inhalation of isoflurane, followed by a transcardial perfusion with ice-cold, oxygenated artificial cerebrospinal fluid (ACSF) containing (in mM) 127 NaCl, 2.5 KCl, 25 $NaHCO_3$, 1.25 NaH_2PO_4, 2.0 $CaCl_2$, 1.0 $MgCl_2$, and 25 glucose (osmolarity 310 mOsm/L). After perfusion, the brain was rapidly removed, and immersed in ice-cold ACSF equilibrated with 95%O_2/5%CO_2. Tissue was blocked and transferred to a slicing chamber containing ice-cold ACSF, supported by a small block of 4% agar (Sigma-Aldrich). Bilateral 300 µm-thick slices were cut on a Leica VT1000s in a rostro-caudal direction and transferred into a holding chamber with ACSF, equilibrated with 95%O_2/5%CO_2. Slices were incubated at 34°C for 30 min prior to electrophysiological recording. Slices were transferred to a recording chamber perfused with oxygenated ACSF at a flow rate of 2–4 ml/min at room temperature.

To assess the number of action potentials evoked by current injections, current clamp whole-cell recordings were obtained from neurons visualized under infrared DODT or DIC contrast video microscopy using patch pipettes of ~2–5 MΩ resistance. Neurons received 500 ms long, -20 pA to 160 pA current injections (in 20 pA steps), randomized across 15 sec-long sweeps. To assess spontaneous firing rate of dopaminergic neurons in the VTA, cell-attached recordings were performed. Cell-attached recording electrode pipettes were filled with the internal solution for voltage clamp recordings, with pipette resistance varying between 3 and 7 MΩ. Dopaminergic neurons were identified by the expression of mCherry in DAT^{iCre} mice. To activate ChR2-expressing fibers of VTA DA neurons in the mPFC, 2 ms-long light pulses (470 nm, ~2 mW) at intervals of 30 sec were delivered at the recording site using whole-field illumination through a 60X water-immersion objective (Olympus, Tokyo, Japan) with a PE4000 CoolLED illumination system (CoolLED Ltd., Andover, UK). Voltage clamp whole-cell recordings were performed to measure light-evoked excitatory postsynaptic currents (EPSCs) in the presence of 10 µM gabazine. Recording electrodes contained the following (in mM): Current-clamp recordings: 135 K-gluconate, 4 KCl, 10 HEPES, 10 Na-phosphocreatine, 4 MgATP, 0.4 Na_2GTP, and

1 EGTA (pH 7.2, 295 mOsm/L). Voltage clamp and cell-attached recordings: 120 $CsMeSO_4$, 15 CsCl, 10 HEPES, 10 Na- phosphocreatine, 2 MgATP, 0.3 NaGTP, 10 QX314, and 1 EGTA (pH 7.2-7.3, ~295 mOsm/L). Recordings were made using 700B amplifiers (Axon Instruments, Union City, CA); data were sampled at 10 kHz and filtered at 4 kHz with a MATLAB-based acquisition script (MathWorks, Natick, MA). Series resistance and input resistance were monitored using a 250 ms, 5 mV hyperpolarizing pulse at every sweep, and experiments were started after series resistance had stabilized (~20 MΩ, uncompensated). Offline analysis of electrophysiology data was performed using Igor Pro (Wavemetrics, Portland, OR) and MATLAB (Mathworks, Natick, MA).

Two-photon imaging with two-photon glutamate uncaging

Dendritic imaging and uncaging of MNI-glutamate for spinogenesis induction were accomplished on a custom-built microscope combining two-photon laser-scanning microscopy (2PLSM) and two-photon laser photoactivation, as previously described[40,41,54]. Two mode-locked Ti:Sapphire lasers (Mai Tai eHP and Mai Tai eHP DeepSee, Spectra-Physics, Santa Clara, CA) were tuned to 910 and 725 nm for exciting EGFP and uncaging MNI-glutamate, respectively. The intensity of each laser was independently controlled by Pockels cells (Conoptics, Danbury, CT). A modified version of Scanimage software was used for data acquisition [78]. For glutamate uncaging, 2.5 mM MNI-caged-L-glutamate (Tocris) was perfused into the slice chamber, and 725 nm light guided through a galvo scanhead was used to focally release the caging group. Secondary and tertiary dendritic branches were selected for dendritic imaging and spinogenesis induction. MNI-glutamate was uncaged near the dendrite (~0.5 µm) at 2 Hz using up to forty 2 ms-long pulses. Images were continually acquired during the induction protocol at 1 Hz, and uncaging was stopped if a spinehead was visible before 40 uncaging pulses were delivered. Analysis was carried out on raw image stacks and z projections. For display purposes only, a subset of the 2-photon micrographs was processed using Candle[80]. A successful induction of new dendritic spine was scored when an obvious protrusion from the dendrite in the uncaging location was observed. For each animal, the probability of spinogenesis is represented as the fraction of successful induction trials out of all trials, ($P(spinogenesis) = number\ of\ succesful\ trials/total\ number\ of\ trials$).

Pharmacology

Pharmacological agents were acquired from Tocris (Bristol, UK) or Sigma-Aldrich (St. Louis, MO). *In vivo* injections included intraperitoneal and subcutaneous injections of ketamine (10 mg/kg, Vedco, St. Joseph, MO), SKF 83566 (10 mg/kg, Tocris), Clozapine N-oxide (3 mg/kg *in vivo*, 1 µM *in vitro*, Sigma-Aldrich). SR 95531 hydrobromide was used in acute slice experiments, as noted (gabazine, 10 µM, Tocris).

Tissue processing and immunohistochemistry

Mice were deeply anaesthetized with isoflurane and transcardially perfused with 4% paraformaldehyde (PFA) in 0.1 M phosphate buffered saline (PBS). Brains were post-fixed for 1-5 days and washed in PBS, prior to sectioning at 50-100 µm on a vibratome (Leica Instruments, Nussloch, Germany). No immunoenhancement was used to increase the signal of virally transduced fluorescent proteins. Sections were pretreated in 0.2% Triton X-100 for an hour at RT, then blocked in 10% bovine serum albumin (BSA, Sigma-Aldrich, ST Louis, MO):PBS with 0.05% Triton X-100 for two hours at RT, and incubated for 24-48 hrs at 4°C with primary antibody solution in PBS with 0.2% Triton X-100. On the following day, tissue was rinsed in PBS, reacted with secondary antibody for 2 hrs at RT, rinsed again, then mounted onto Superfrost Plus slides (ThermoFisher Scientific, Waltham, MA). Sections were dried and coverslipped under ProLong Gold antifade reagent with DAPI (Molecular Probes, Life Technologies, Carlsbad, CA) or under glycerol:TBS (3:1) with Hoechst 33342 (1:1000; ThermoFisher Scientific). Primary antibodies used in the study were rabbit anti-tyrosine hydroxylase

(1:1000; AB152, Abcam, Cambridge, UK), chicken anti-GFP (1:2000; AB13970, Abcam, Cambridge, UK), rabbit anti-RFP (1:500, 600-401-379, Rockland, Limerick, PA), and rabbit anti-c-Fos (1:5000; Synaptic Systems, Goettingen, Germany). Alexa Fluor 488- or Fluor 647-conjugated secondary antibodies against rabbit or chicken (Life Technologies, Carlsbad, CA) were diluted 1:500. Whole sections were imaged with an Olympus VS120 slide scanning microscope (Olympus Scientific Solutions Americas, Waltham, MA). Confocal images were acquired with a Leica SP5 confocal microscope (Leica Microsystems). Depth-matched z-stacks of 2 µm-thick optical sections were analyzed in ImageJ (FIJI) [81]. For c-fos quantification, every four adjacent z stack slices were combined, for a total of 6 µm thickness. mCherry signal was used to localize cell bodies of hM3Dq-expressing neurons. Laser intensity was held constant across all c-fos samples, and the same threshold was applied for subtracting background immunofluorescence. C-fos$^+$ positive neurons were identified by an experimenter blind to the conditions.

Quantitative fluorescence *in situ* hybridization

Quantitative fluorescence *in situ* hybridization (FISH) was conducted following previously published procedures[62,79]. Mice were deeply anesthetized by inhalation of isoflurane and decapitated. Brains were quickly removed and frozen in tissue-freezing medium on a mixture of dry ice and ethanol for 5 - 15 min prior to storage at 80°C. Brains were subsequently cut on a cryostat (Leica CM1850) into 20 µm-thick sections, adhered to Superfrost Plus slides, and frozen at 80°C. Samples were fixed with 4% PFA in 0.1 M PBS at 4°C for 15 min, processed according to the manufacturer's instructions in the RNAscope Fluorescent Multiplex Assay manual for fresh frozen tissue (Advanced Cell Diagnostics, Newark, CA), and coverslipped with ProLong Gold antifade reagent with DAPI (Molecular Probes). Enhanced green fluorescent protein channel 1 (*Egfp*) and dopamine Drd1a receptor channel 2 (*Drd1a*) probes were added to slides in combination, and Amp4-b fluorescent amplification reagent was used for all experiments. Sections were subsequently imaged on a Leica SP5 confocal microscope in four channels with a 40x objective lens at a zoom of 1.4 and resolution of 512 x 512 pixels with 1.0 µm between adjacent z sections. Images were taken across the entirety of the population of *Egfp*-positive neurons in each brain section.

FISH images were analyzed using FIJI[81]. Briefly, every four adjacent z stack slices were combined, for a total of 3 µm thickness, in order to minimize missed colocalization, while minimizing false positive colocalization driven by signal from cells at a different depth in a similar x-y position. All channels were thresholded. Cellular ROIs were defined using the *Egfp*$^+$ or retrobead$^+$ channel information to localize cell bodies. FISH molecule puncta were counted within established cell boundaries. Whether a cell was considered positive for a given marker was determined by setting a transcript-dependent threshold of the number of puncta (e.g., over 5 puncta/soma for *Drd1a*$^+$). These stringent parameters for co-localization and the challenges of quantifying low abundance receptor transcripts likely lead to underestimation of receptor-positive population sizes.

Quantification of behavior

For evaluating locomotor behavior, Toxtrac[82] was used to track the animal's position, defined by its body center position, and quantify the distance travelled in each session. To detect motion onset/offset, movement was defined by the body center moving > 30 mm/sec for at least 0.5 sec. The associated Ca^{2+} transients were then aligned to transitions between motion start and stop times and averaged across all animals.

Three state transition models were constructed for a given condition and behavioral response, by counting the occurrence of each of the 3 possible 2-response sequences in all animals and then dividing by the total number of the given response. For example, an escape can be followed by another escape, a failure, or a premature trial. The probability of a failure following an escape was calculated by counting the number of failures that followed escapes and dividing it by the total number of escape trials. The similarity between

transition models was calculated as one minus the Frobenius norm (the Euclidean norm of a matrix) of the difference between models ($1 - norm(model_a - model_b)$). To depict individual learning trajectories, starting at zero, trajectory value incremented by 1 for each escape trial, decremented by 1 for each failure trial, and kept constant for premature (spontaneous transitions in the shuttle box) trials. The slope of the behavioral response curves was obtained by performing a least-squares fit of a line to a given segment (Baseline or LH + KET) using the Numpy polyfit function in Python.

Quantification of fiber photometry data

The heatmap of Ca^{2+} transients was constructed by plotting single trial transients with signal amplitude depicted by color. The latency to peak was defined as the time from stimulus onset to the maximum Ca^{2+} transient value within 8 sec of stimulus onset. The negative and positive area under the curve (AUC) was calculated based on the direction of the peaks. Peaks that are less than 5% of the distance from minimum to maximum dF/F were omitted from analyses. The baseline was chosen by using the mean dF/F of the 5 sec segment before the shock onset. For behavioral response-specific Ca^{2+} transients, the transients for each behavioral response were averaged within a single subject, and then these data were averaged across all animals. For Ca^{2+} traces corresponding to successful escapes, stimulus length varies according to escape latency. The distance between escape and failure traces for each animal was computed as the Euclidean norm of the difference between the average of all their Ca^{2+} transients on escape trials and the average of all their Ca^{2+} transients on failure trials ($||escape - failure||_2$).

Statistical analyses

Group statistical analyses were done using GraphPad Prism 7 software (GraphPad, LaJolla, CA). For N sizes, the number of trials or cells recorded, as well as the number of animals are provided. All data are expressed as mean + SEM, or individual plots. Probabilities are expressed as aggregate probabilities across experiments of the same type. For two-group comparisons, statistical significance was determined by two-tailed Student's t-tests or two-sample Z test for proportions. For multiple group comparisons, one-way analysis of variance (ANOVA) tests were used for normally distributed data, followed by post hoc analyses. For non-normally distributed data, non-parametric tests for the appropriate group numbers were used. Pearson regression was used to detect the correlation between two groups of data. $P < 0.05$ was considered statistically significant.

Figures and Legends

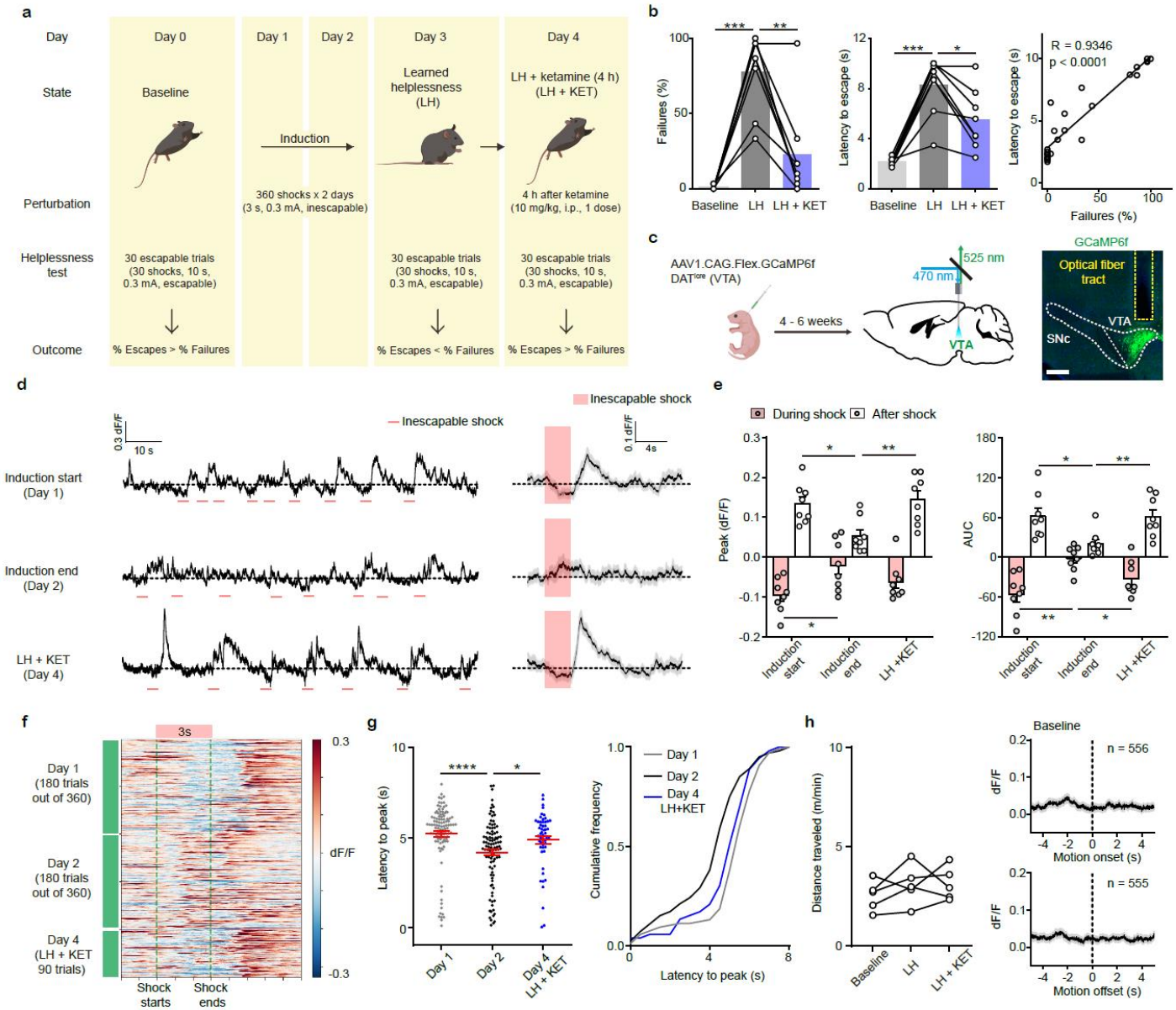

Figure 1. Ketamine rescues escape behavior and dampened DA neuronal activity after aversive learning

(a). Schematic illustrating the task and the evaluation of behavioral outcomes.

(b). Left, summary data showing the percentage of failures to escape an escapable aversive stimulus across phases of learning (Baseline, LH, and LH + KET). Middle, same as left, but for latency to escape. Right, for all conditions, the correlation between percentage of failure to escape and escape latency (failure to escape trials scored as 10 sec latency). n = 8 mice. Failures: repeated measures one-way ANOVA, $F(1.89, 13.23) = 27.9$, $p = 0.0001$, Sidak's multiple comparison test, Baseline vs LH, $p = 0.0001$, LH vs LH+KET, $p = 0.0037$. Latency to escape: repeated measure one-way ANOVA, $F(1.96, 13.72) = 29.63$, $p < 0.0001$, Sidak's multiple

comparison test, Baseline vs LH, $p = 0.0003$, LH vs LH+KET, $p = 0.0141$. Pearson correlation: $R = 0.9346$, $p < 0.0001$.

(c). Left, schematic for viral transduction in the VTA and subsequent fiber implant. Right, fiber placement verification. Green, GCaMP6f; blue, Hoechst nucleic stain. Scale bar: 500 µm.

(d). Left, baseline adjusted raw traces of VTA DA neuron Ca^{2+} responses to inescapable foot-shocks (3 sec, pink) in one animal at the start of induction, at the end of induction, and 4 hrs following a single dose of ketamine (LH + KET, 10 mg/kg i.p.). Right, average traces in the same subject aligned to stimulus start time (20 trials/condition, mean ± SEM).

(e). Left, quantification of peak Ca transient amplitude during and after foot-shock stimuli across conditions. Right, same but for area under the curve (AUC). Both positive and negative values are quantified. $n = 8$ animals, repeated measures one-way ANOVA, Holm-Sidak's multiple comparison test, Peak: During shock, $F(1.823, 12.76) = 5.387$, $p = 0.0222$, Induction start vs Induction end, $p = 0.0458$, Induction end vs LH+KET, $p = 0.0788$. After shock, $F(1.693, 11.85) = 6.805$, $p = 0.0132$, Induction start vs Induction end, $p = 0.0230$, Induction end vs LH+KET, $p = 0.0068$. AUC: During shock, $F(1.705, 11.94) = 8.942$, $p = 0.0054$, Induction start vs Induction end, $p = 0.0058$, Induction end vs LH+KET, $p = 0.0258$. After shock, $F(1.437, 10.06) = 5.499$, $p = 0.0318$, Induction start vs Induction end, $p = 0.0257$, Induction end vs LH+KET, $p = 0.0069$. (f). Heatmap of single trial Ca^{2+} traces across learning in one mouse (Day 1, induction day 1; day 2, induction day 2; day 4, LH + KET). Pink rectangle and green dashed lines mark the timing of shock stimuli. Colormap of dF/F, blue -0.3, red 0.3, saturated for values outside this range for illustration purposes.

(g). Left, latencies from stimulus onset to dF/F peak (averages of sequential bins of 10 traces) for all subjects across learning days as described in (F). Right, cumulative frequency distribution of latencies to peak. $n = 6$ animals, one-way ANOVA, $F(2, 258) = 9.387$, $p = 0.0001$. Sidak's multiple comparison test, Day 1 vs Day 2, $p = 0.0001$, Day 2 vs LH+KET, $p = 0.0342$.

(h). Left, open field locomotion (m/min) for several mice across learning phases. Right top, average of Ca^{2+} transients (mean ± SEM) around motion onset ($n = 556$ events) for mice in the baseline condition. Right bottom, same but for motion offset ($n = 555$ events). Dashed black line marks motion onset/offset. $n = 5$ animals, repeated measures one-way ANOVA, $F(1.038, 4.153) = 1.479$, $p = 0.2910$.

*$p < 0.05$, ** $p < 0.01$, *** $p < 0.001$, **** $p < 0.0001$.

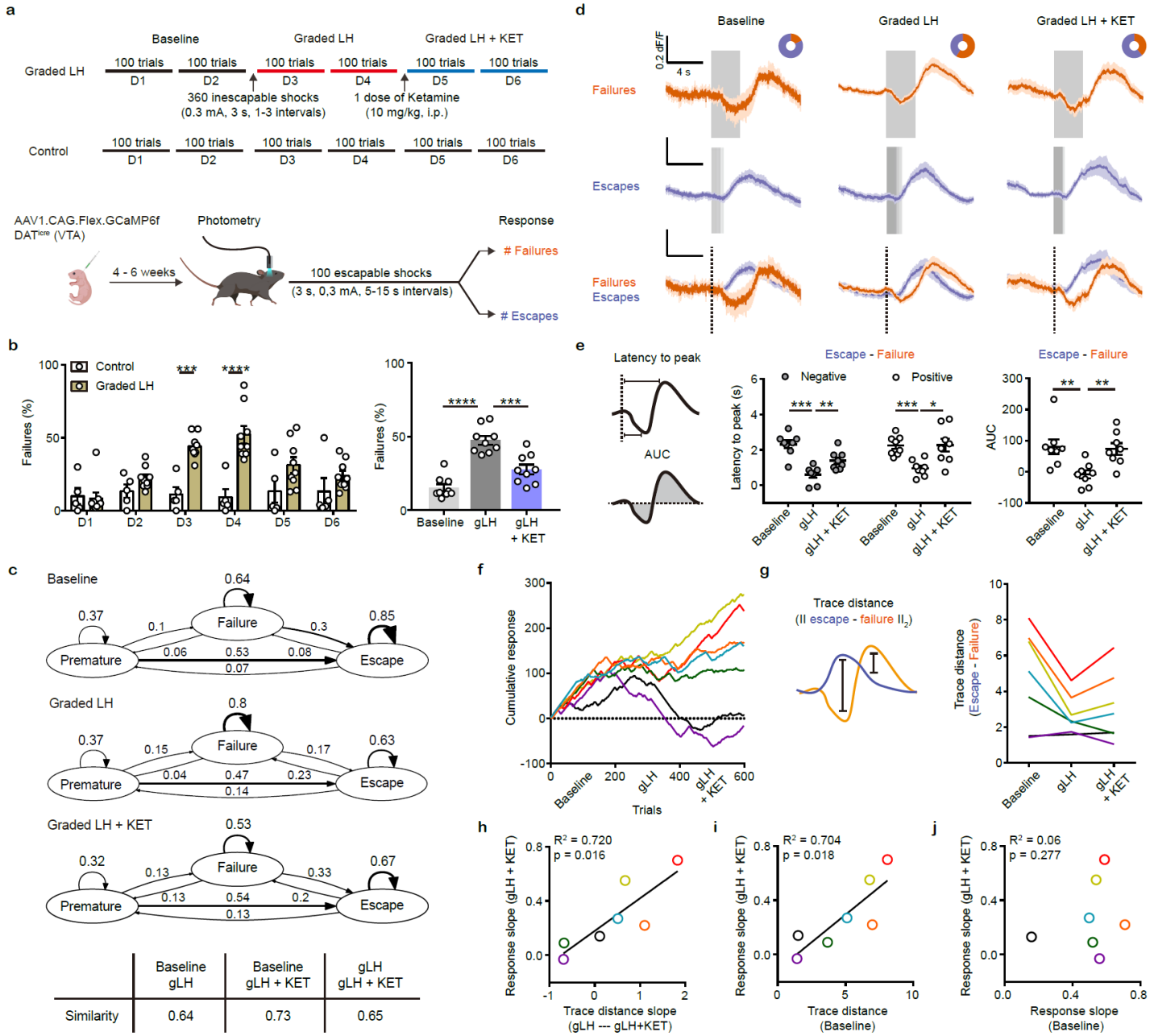

Figure 2. Graded learning analysis uncovers links between DA activity features, behavioral outcomes, and response to ketamine

(a). Top, schematic of experimental timeline for graded LH (gLH). Bottom, schematic of viral transduction and timing of photometry recording.

(b). Left, summary data showing the percentage of failures to escape an escapable aversive stimulus across 6 days for two groups (white bar, controls; beige, gLH). Right, within group summary of behavioral data for gLH mice across learning phases. Control, n = 5 mice, gLH, n = 9 mice. Left, responses across days, two-way ANOVA, Sidak's multiple comparison test, Control vs gLH, D3, $p = 0.0002$, D4, $p < 0.0001$, D5, $p = 0.103$, D1, D2, and D6, $p > 0.6$. Right, repeated measures one-way ANOVA, $F(1.908, 15.26) = 66.15$, $p < 0.0001$. Sidak's multiple comparison test, Baseline vs gLH, $p < 0.0001$, gLH vs gLH + KET, $p = 0.0001$.

(c). Graphs depicting transition probabilities between behavioral responses during baseline (top), gLH (middle), and gLH + KET (bottom). Arrow sizes are proportional to transition probability, noted numerically. Table, Frobenius norms of differences between graphs for each graph pair. n = 7 animals, 1400 trials/condition.

(d). Fiber photometry recordings of VTA DA Ca^{2+} transients, separated by behavioral response and aligned to shock start time (purple, escape; orange, failure; average dF/F across all animals). Grey rectangles mark stimulus length in time, which is constant for failures to escape but variable for successful escapes and is shaded proportionally. Donut plots depict proportion of behavioral responses. n = 8 animals, baseline: 1420 trials, 18% failure 82% escape; gLH: 1370 trials, 59% failure 41% escape; gLH + KET: 1174 trials, 39% failure, 61% escape.

(e). Left, schematic illustration for measured variables. Middle, summary data for differences in the latency to negative (grey) and positive (white) Ca^{2+} transient peaks across learning phases. Right, same but for absolute value of AUC, as shown in the schematic. n = 8 mice, Latency to trough (negative peak), repeated measures one-way ANOVA, $F(1.746, 12.22) = 26.22$, $p < 0.0001$, Holm-Sidak's multiple comparison test, Baseline vs gLH, $p = 0.0008$, gLH vs gLH + KET, $p = 0.0041$. Latency to positive peak, repeated measures one-way ANOVA, $F(1.198, 8.389) = 12.52$, $p = 0.0057$, Holm-Sidak's multiple comparison test, Baseline vs gLH, $p = 0.0002$, gLH vs gLH + KET, $p = 0.0127$. AUC, repeated measures one-way ANOVA, $F(1.471, 10.3) = 13.68$, $p = 0.0021$, Holm-Sidak's multiple comparison test, Baseline vs gLH, $p = 0.0088$, gLH vs gLH + KET, $p = 0.0088$

(f). Learning curves for individual animals with subject-specific colors maintained across panels F-J. n = 7 animals, 600 trials/animal.

(g). Left, schematic illustration for the measured variable, Euclidean norm of the difference between mean escape and failure-associated Ca^{2+} transients for each subject. Right, trace distances for each subject across learning phases.

(h). Correlation between the slope of trace distance (gLH to gLH + KET) and the slope of the learning curve in gLH + KET.

(i). Correlation between trace distance in the baseline condition and the slope of the learning curve in gLH + KET.

(j). Correlation between the slope of the learning curve in the baseline condition and the slope of the learning curve in gLH + KET.

*$p < 0.05$, ** $p < 0.01$, *** $p < 0.001$, **** $p < 0.0001$.

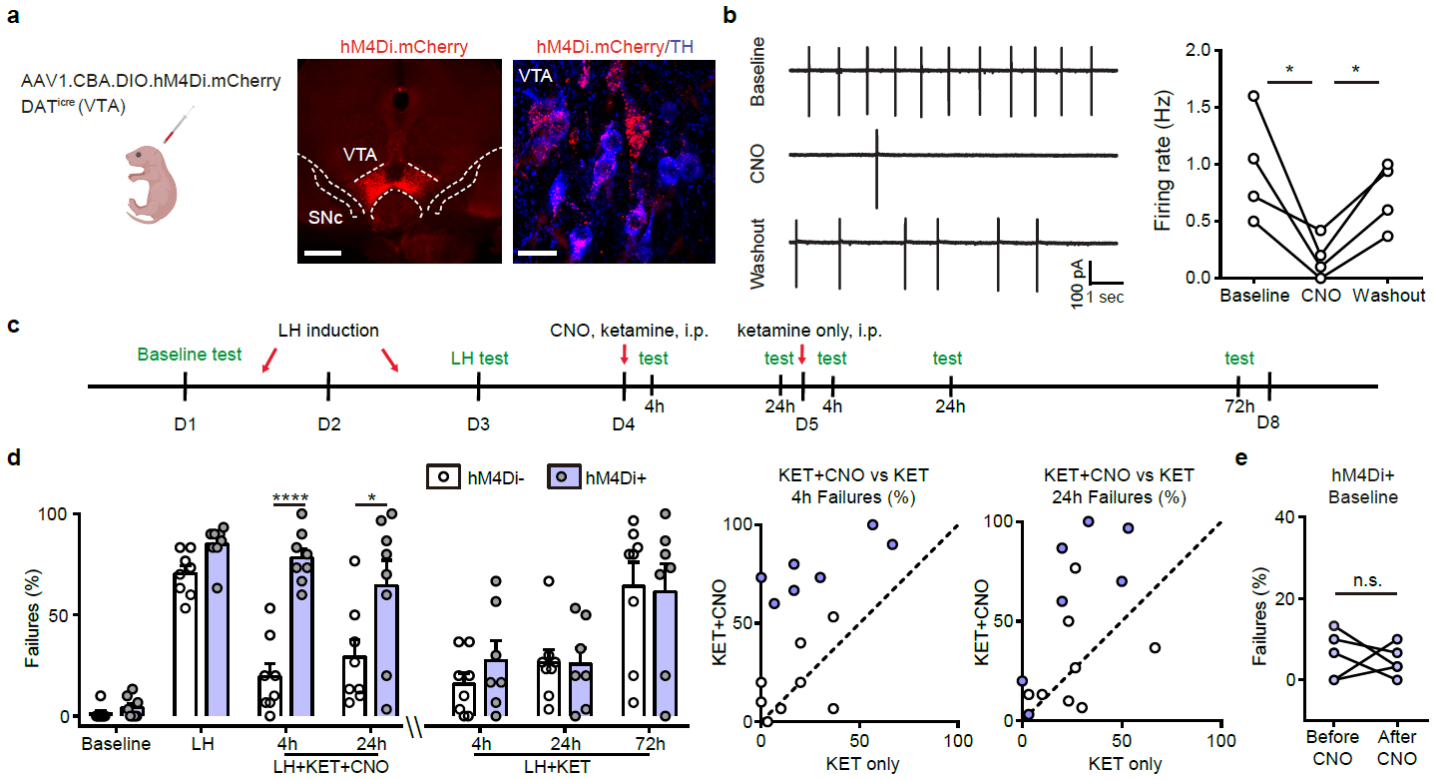

Figure 3. Ketamine behavioral effects require VTA DA activity

(a). Schematic for viral transduction in the VTA and hM4Di expression in VTA DA neurons (red, hM4Di.mCherry; blue, tyrosine hydroxylase (TH) immunofluorescence). Scale bars, 500 µm and 20 µm.

(b). Cell-attached recording of spontaneous activity in an mCherry^{+} VTA neuron before, during, and after bath application of 1 µM clozapine- N-oxide (CNO). Example traces (left) and summary data (right). n = 4 cells from 3 mice, repeated measures one-way ANOVA, $F_{(2, 6)} = 9.634$, $p = 0.0134$, Sidak's multiple comparison test, Baseline vs CNO, $p = 0.0104$, CNO vs Washout, $p = 0.0488$.

(c). Schematic of experimental timeline and pharmacological interventions.

(d). Left, summary data showing the percentage of failures to escape an escapable aversive stimulus across learning and treatment conditions for hM4Di AAV expressing DAT^{iCre} positive and negative littermates. Middle, within subject summary data for behavioral responses after ketamine treatment only, compared with ketamine + CNO, 4 hrs after treatment. Right, same but for 24 hrs after treatment. Two-way ANOVA, Sidak's multiple comparison test, KET + CNO 4 hrs, $p < 0.0001$, KET + CNO 24 hrs, $p = 0.0107$, KET only, following 4, 24, and 72 hrs, $p > 0.9$.

(e). Summary data showing the percentage of failures to escape an escapable aversive stimulus in the baseline condition, for hM4Di-expressing mice before and after CNO treatment. n = 5 mice, two-tailed paired t-test, $p = 0.7292$.

*$p < 0.05$, ** $p < 0.01$, **** $p < 0.0001$.

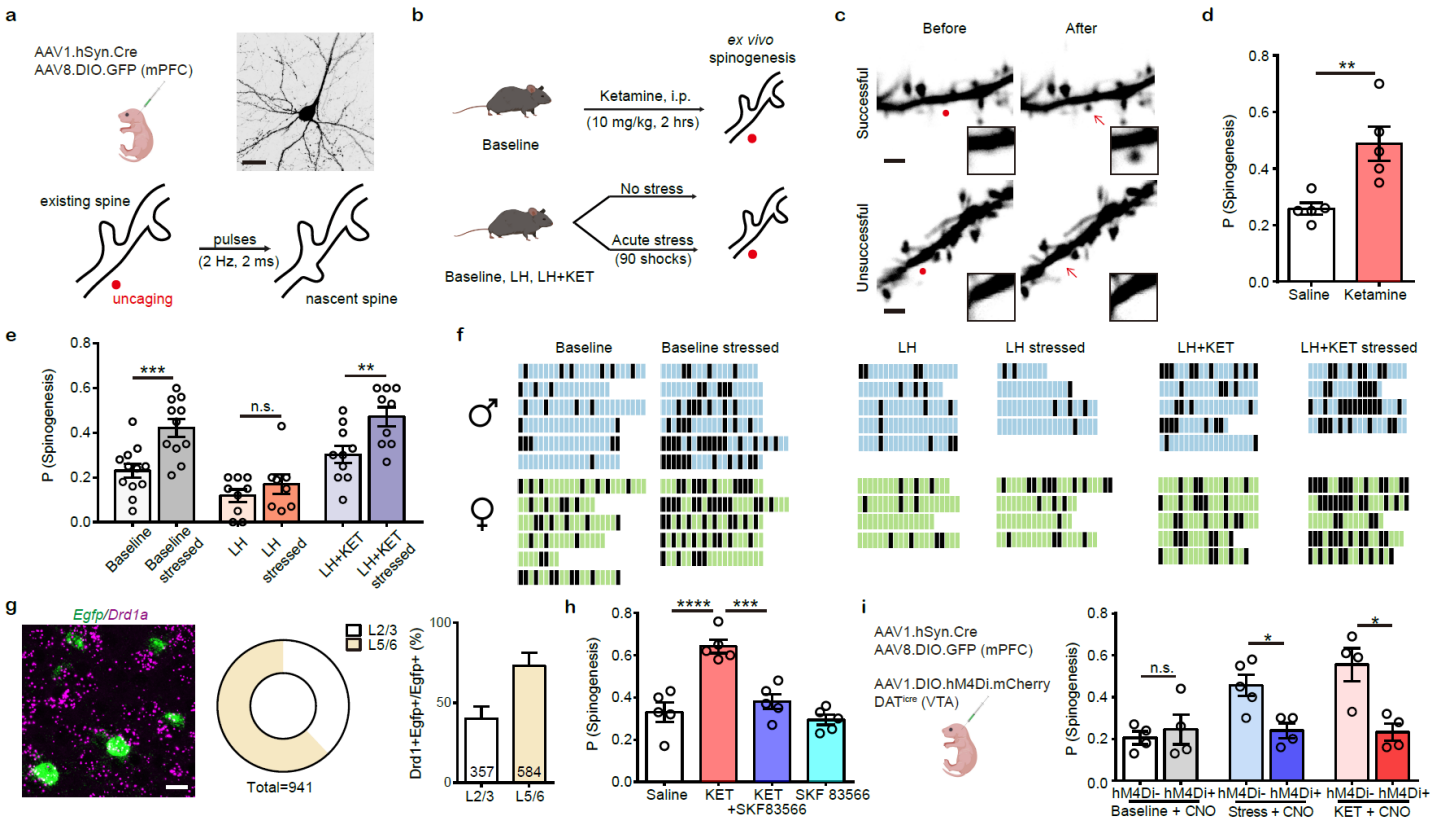

Figure 4. Ketamine rescues mPFC plasticity after aversive experience by altering DA signaling via Drd1 receptors

(a). Schematic illustrating glutamate-evoked *de novo* spinogenesis platform. Top, viral transduction and an example EGFP$^+$ pyramidal neuron in mPFC. Bottom, MNI-glutamate uncaging parameters and the induction of new dendritic spines.

(b). Schematic illustrating experience-driven and pharmacological manipulations.

(c). Example 2PLSM images of successful and unsuccessful induction trials of *de novo* spinogenesis. Red circles, uncaging sites. Black rectangle, close up images of local dendritic segments before and after glutamate uncaging. Scale bar, 2 µm.

(d). Probability of spinogenesis on deep layer mPFC neurons in mice treated with either saline or ketamine (i.p. 10 mg/kg, acute slice preparation 2 hrs after treatment). Each circle, aggregate probability of evoked spinogenesis from a single animal. n = 5 animals, 15-25 trials/animal, Saline, 0.258 ± 0.02. Ketamine, 0.488 ± 0.06. Two-tailed unpaired t-test, p = 0.0073.

(e). Same as D, but for mice in distinct stages of aversive learning (baseline, LH, LH + KET), with or without acute stress. n = 8 - 12 animals/condition as shown in plots, two-tailed unpaired t-test, Baseline vs Baseline stressed, p = 0.0009. LH vs LH stressed, p = 0.0326. LH +KET vs LH + KET stressed, p = 0.0095. One-way ANOVA, F (2, 28) = 7.146, p = 0.0031, Sidak's multiple comparison test, Baseline vs LH, p = 0.0496, LH vs LH + KET, p = 0.0016.

(f). Binary grid plots illustrating sequences of spinogenesis induction outcomes for different mice in all conditions, separated by sex. Black, successful evoked spinogenesis trial; blue or green, unsuccessful trial for males and females, respectively.

(g). Left, fluorescence *in situ* hybridization (FISH) image showing *Drd1a* mRNA in *Egfp* mRNA expressing mPFC cells. Middle, the proportional distribution of *Egfp* mRNA expression across superficial and deep cortical layers. Right, quantification of the percentage of *Drd1a*$^+$ cells among *Egfp*$^+$ cells in superficial and deep cortical layers. n = 4 animals; *Drd1*$^+$*Egfp*$^+$/*Egfp*$^+$: Layer 2/3, 40.2% ± 7.5%, layer 5/6, 73.1% ± 8.3%, mean ± SEM.

(h). Probability of spinogenesis on deep layer mPFC neurons in mice treated with Saline, KET (10 mg/kg), KET + SKF 83566 (10 mg/kg), or SKF 83566 alone. One-way ANOVA, $p < 0.0001$, $F (3, 16) = 20.29$, Sidak's multiple comparison test, Saline vs KET, $p < 0.0001$, KET vs KET + SKF83566, $p = 0.0002$, Saline vs SKF83566, $p = 0.8574$.

(i). Left, schematic illustrating viral transduction strategy. Right, probability of spinogenesis on deep layer mPFC neurons in DAT $^{icre+}$ and DAT $^{icre-}$ animals treated with CNO (3 mg/kg) across conditions (baseline, stress, and KET). n = 4 - 5 animals/condition as shown in plots, two-tailed unpaired t-test, Cre$^+$ vs Cre$^-$, CNO, $p = 0.6245$. Stress + CNO, $p = 0.0132$. KET + CNO, $p = 0.0103$.

*$p < 0.05$, ** $p < 0.01$, *** $p < 0.001$, **** $p < 0.0001$.

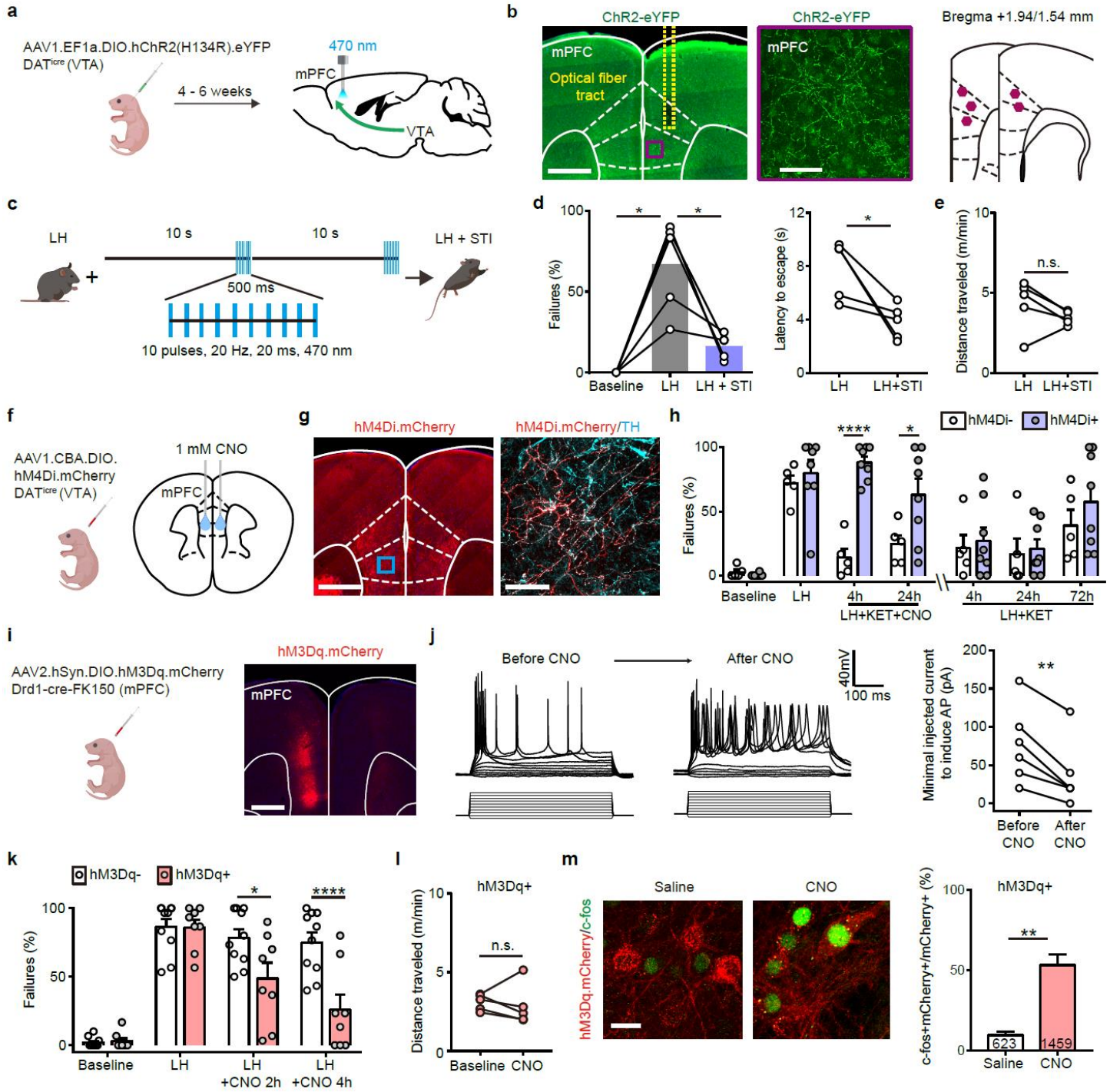

Figure 5. Activity of local DA terminals and Drd1⁺ neurons in mPFC mediates behavioral responses to ketamine

(a). Left, schematic for viral transduction with Cre-dependent ChR2 AAV in the VTA and subsequent optogenetic fiber implant in mPFC.

(b). Left, fiber placement illustration on a coronal section through mPFC, with a close up image of ChR2.eYFP terminals (white dashed lines, Paxinos atlas overlay; yellow dashed lines, fiber track). Green,

immunoenhanced ChR2.eYFP; blue, Hoechst nucleic stain. Scale bars: 500 μm and 50 μm. Right, atlas location of fiber placement for each subject.

(c). Schematic illustrating optogenetic stimulation parameters, delivered without time-locking to shocks (STI denotes optogenetic stimulation).

(d). Left, summary data showing the percentage of failures to escape an escapable aversive stimulus in ChR2-expressing mice across phases of learning, Baseline, LH, and LH + STI. Right, summary data for latency to escape in LH compared with LH + STI conditions. n = 5 animals, Failures, repeated measures one-way ANOVA, F (1.041, 4.163) = 17.95, p = 0.0120, Holm-Sidak's multiple comparison test, Baseline vs LH, p = 0.0125, LH vs LH + STI, p = 0.0295. Latency to escape, two-tailed paired t-test, p = 0.0329.

(e). Left, open field locomotion (m/min) for several mice after learning with and without optogenetic stimulation. Two-tailed paired t-test, p = 0.2079, n = 5 mice.

(f). Left, schematic illustrating viral transduction strategy. Right, local CNO infusion in mPFC (1 mM, 1 μl).

(g). Left, immunoenhanced image of hM4Di.mCherry^{+} DAT^{+} terminals in mPFC. Right, mCherry^{+} terminals colocalize with a subset of tyrosine hydroxylase (TH) expressing axons. Scale bars, 500 μm and 50 μm.

(h). Summary data showing the percentage of failures to escape an escapable aversive stimulus across learning and treatment conditions for hM4Di-expressing DAT^{iCre} positive and negative littermates. n = 5 mice for Cre^{-}, 8 mice for Cre^{+}, two-way ANOVA, Sidak's multiple comparison test. KET + CNO 4 hrs, p < 0.0001, KET + CNO 24 hrs, p = 0.0476, KET + only 4, 24, and 72 hrs, p > 0.7.

(i). Left, schematic illustrating viral transduction strategy. Right, hM3Di-mCherry expression in mPFC. Scale bar, 500 μm.

(j). Whole-cell recording of action potentials evoked by different amplitude current injections in one mCherry^{+} mPFC neuron before, during, and after bath application of 1 μM CNO. Left, example traces. Right, summary data for minimal injected currents sufficient to evoke action potential firing before and after CNO application. n = 6 cells from 2 animals, two-tailed paired t-test, p = 0.0028.

(k). Summary data showing the percentage of failures to escape an escapable aversive stimulus in DAT^{icre+} and DAT^{icre-} mice across phases of learning and after CNO treatment (Baseline, LH, LH + CNO 2 hrs, and LH + CNO 4 hrs). n = 8 mice for Cre^{-}, n = 10 micer for Cre^{+}, two-way ANOVA, Sidak's multiple comparison test, LH + CNO 2 hrs, p = 0.0157, LH + CNO 4 hrs, p <0.0001.

(l). Total distance traveled per minute in an open field locomotion assay for hM3Dq^{+} animals before and after CNO treatment. Two-tailed paired t-test, p = 0.6289.

(m). Left, colocalization of c-fos immunolabeling in mCherry^{+} mPFC neurons in saline and CNO treated Drd1 Cre^{+}, hM3Dq-expresing mice. Right, the quantification of percentage of c-fos^{+} cells among mCherry^{+} cells. Scale bar, 20 μm. n = 3 mice/condition, two-tailed unpaired t-test, p = 0.0031.

*p < 0.05, ** p < 0.01, **** p < 0.0001.

Extended Data Figures and Figure Legends

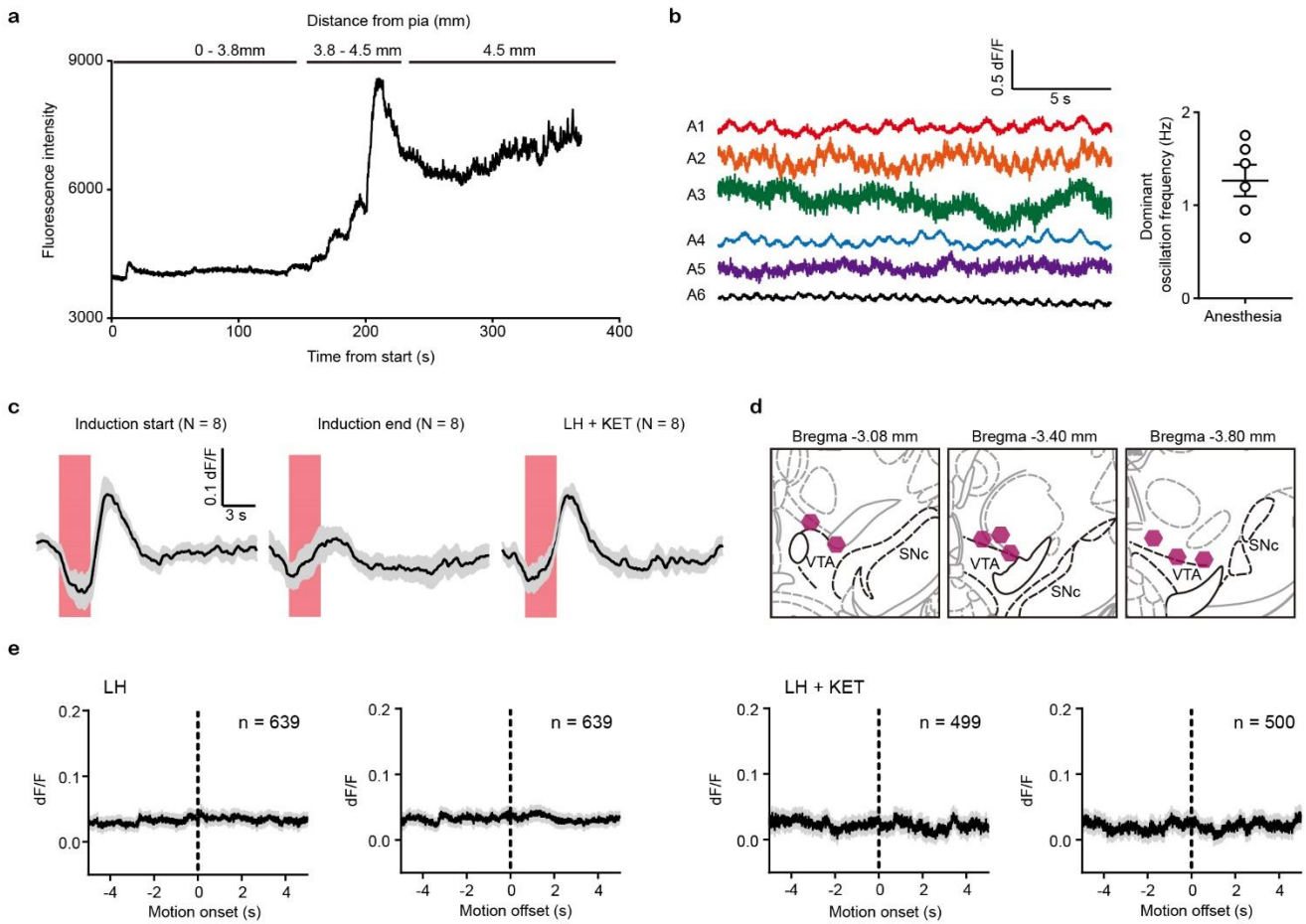

Extended Data Figure 1. VTA DA neuron responses to anesthesia, foot-shock, and motion transitions

(a). Photometry guided fiber implantation into the VTA. Recording starts when the fiber traverses the pia. A gradual increase of fluorescence intensity was observed when the fiber tip approached GCaMP6f-expressing neurons, 3.8 – 4.5 mm from the pia, followed by a sharp signal increase and stabilization close to the VTA.

(b). Oscillation of VTA DA Ca^{2+} transients under anesthesia. Approximately 1-2 Hz oscillations were observed in every animal. Summary data show the dominant oscillation frequencies.

(c). Average Ca^{2+} transients (mean ± SEM) in response to foot-shocks for all animals across learning phases. Traces are aligned to stimulus start time (20 trials/animal, 8 animals).

(d). Atlas locations showing fiber placements for data in Figure 1.

(e). Average Ca^{2+} transients (mean ± SEM) around motion onset and offset for mice in the LH/LH + KET condition. Dashed black line marks motion onset/offset. The number of onsets/offsets, as noted.

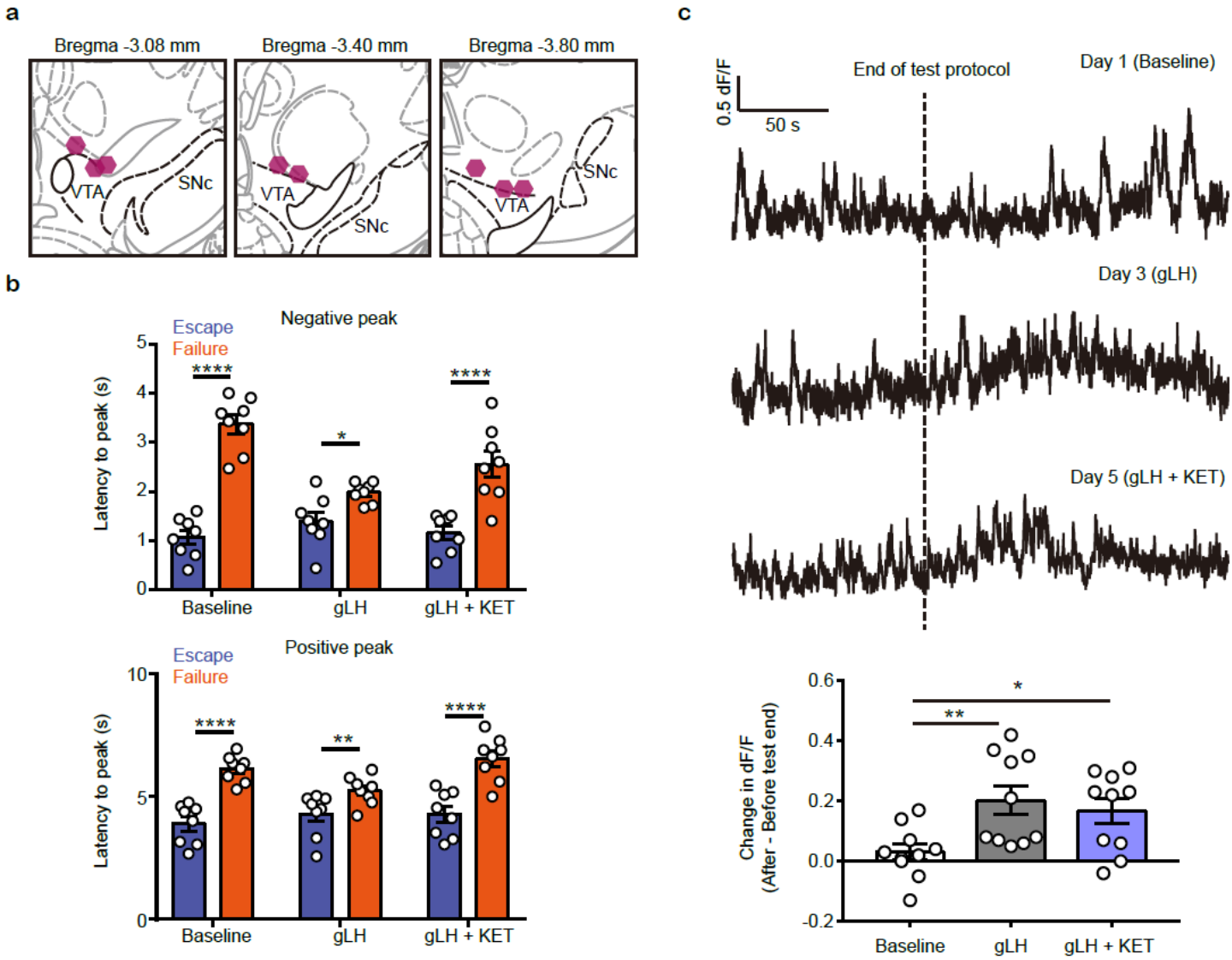

Extended Data Figure 2. VTA DA responses in graded learned helplessness (gLH) paradigm

(a). Atlas locations showing fiber placements for data in Figure 2.

(b). Top, the latency to negative Ca^{2+} transient peaks in escape and failure actions across learning phases. Bottom, the latency to positive Ca^{2+} transient peaks in escape and failure actions across learning phases. Two-way ANOVA, Negative peak, Sidak's multiple comparison test, escape vs failure, Baseline, Mean $\text{difference}_{(\text{failure-escape})}$ = 2.309, $p < 0.0001$, gLH, Mean difference = 0.59, $p = 0.0103$, gLH + KET, Mean difference = 1.39, $p < 0.0001$. Positive peak, Sidak's multiple comparison test, escape vs failure, Baseline, Mean difference = 2.241, $p < 0.0001$, gLH, Mean difference = 0.9565, $p = 0.0014$, gLH + KET, Mean difference = 2.263, $p < 0.0001$.

(c). Increase of overall fluorescent intensity after the end of gLH procedure across learning phases. Top, representative traces from the same subject in each condition. Bottom, summary data for post-trial increases in fluorescent intensity. One-way ANOVA, $F(2, 27) = 5.233$, $p = 0.012$, Sidak's multiple comparison test, Baseline vs gLH, $p = 0.0097$, Baseline vs gLH + KET, $p = 0.044$).

*$p < 0.05$, ** $p < 0.01$, *** $p < 0.001$, **** $p < 0.0001$.

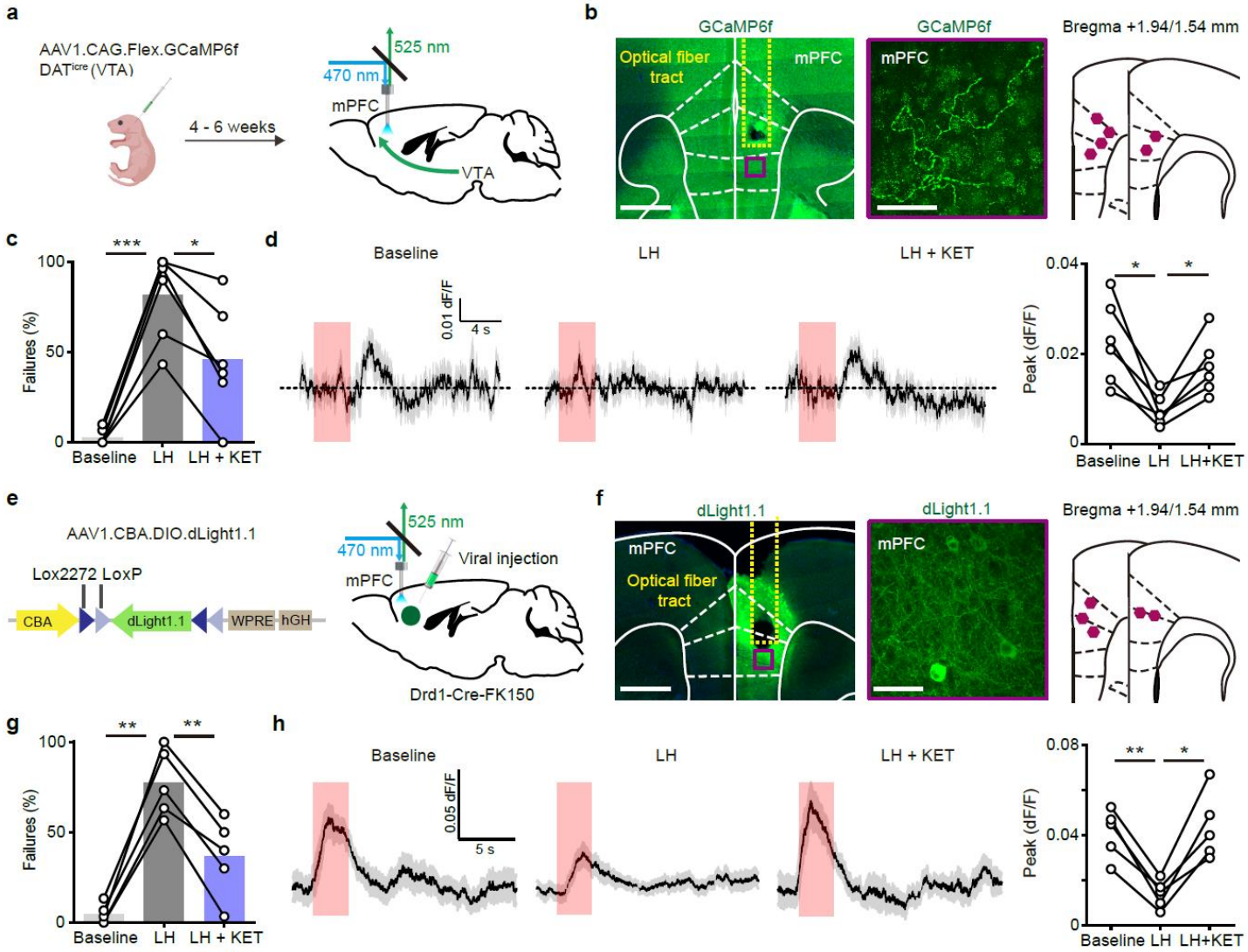

Extended Data Figure 3. DA terminal activity and DA release in mPFC vary across behavioral states

(a). Left, schematic for viral transduction in the VTA and subsequent fiber implant in mPFC.

(b). Left, fiber placement illustration on a coronal section through mPFC, with a close up image of DAT^+ axons (white dashed lines, Paxinos atlas overlay; yellow dashed lines, fiber track). Green, immunoenhanced GCaMP6f; blue, Hoechst nucleic stain. Scale bars: 500 µm and 50 µm. Right, atlas location of fiber placement for each subject.

(c). Summary data showing the percentage of failures to escape an escapable aversive stimulus in GCaMP6f-expressing mice across phases of learning (Baseline, LH, and LH + KET). n = 6 animals, repeated measures one-way ANOVA, F (1.737, 8.684) = 33.44, p = 0.0001, Sidak's multiple comparison test, Baseline vs LH, p = 0.0006, LH vs LH + KET, p = 0.0161.

(d). Left, average Ca^{2+} traces from mPFC DA terminals in one mouse, aligned to stimulus start time across learning phases (20 trials/condition, mean ± SEM; stimulus length, 3 sec, pink shading). Right, within subject group data. Repeated measures one-way ANOVA, F (1.48, 7.401) = 10.71, p = 0.0087, Sidak's multiple comparison test, Baseline vs LH, p = 0.0135, LH vs LH + KET, p = 0.0150.

(e). AAV1.CBA.DIO.dLight1.1 construct and the schematic for viral transduction in the mPFC with subsequent fiber implant in Drd1-Cre-FK150 mice.

(f). Left, fiber placement illustration on a coronal section through mPFC, with a close up image of dLight1.1^{+} neurons and terminals (white dashed lines, Paxinos atlas overlay; yellow dashed lines, fiber track). Green, immunoenhanced dLight1.1; blue, Hoechst nucleic stain. Scale bars: 500 μm and 50 μm. Right, atlas location of fiber placement for each subject.

(g). Same as C, but for dLight1.1-expressing mice. n = 5 animals, repeated measures one-way ANOVA, F (1.434, 5.735) = 51.75, p = 0.0003, Sidak's multiple comparison test, Baseline vs LH, p = 0.0010, LH vs LH + KET, p = 0.0023.

(h). Same as D, but for dLight1.1 transients in mPFC. Repeated measures one-way ANOVA, F (1.693, 6.773) = 24.16, p = 0.001, Sidak's multiple comparison test, Baseline vs LH, p = 0.0036, LH vs LH + KET, p = 0.0107.

*p < 0.05, ** p < 0.01, *** p < 0.001.

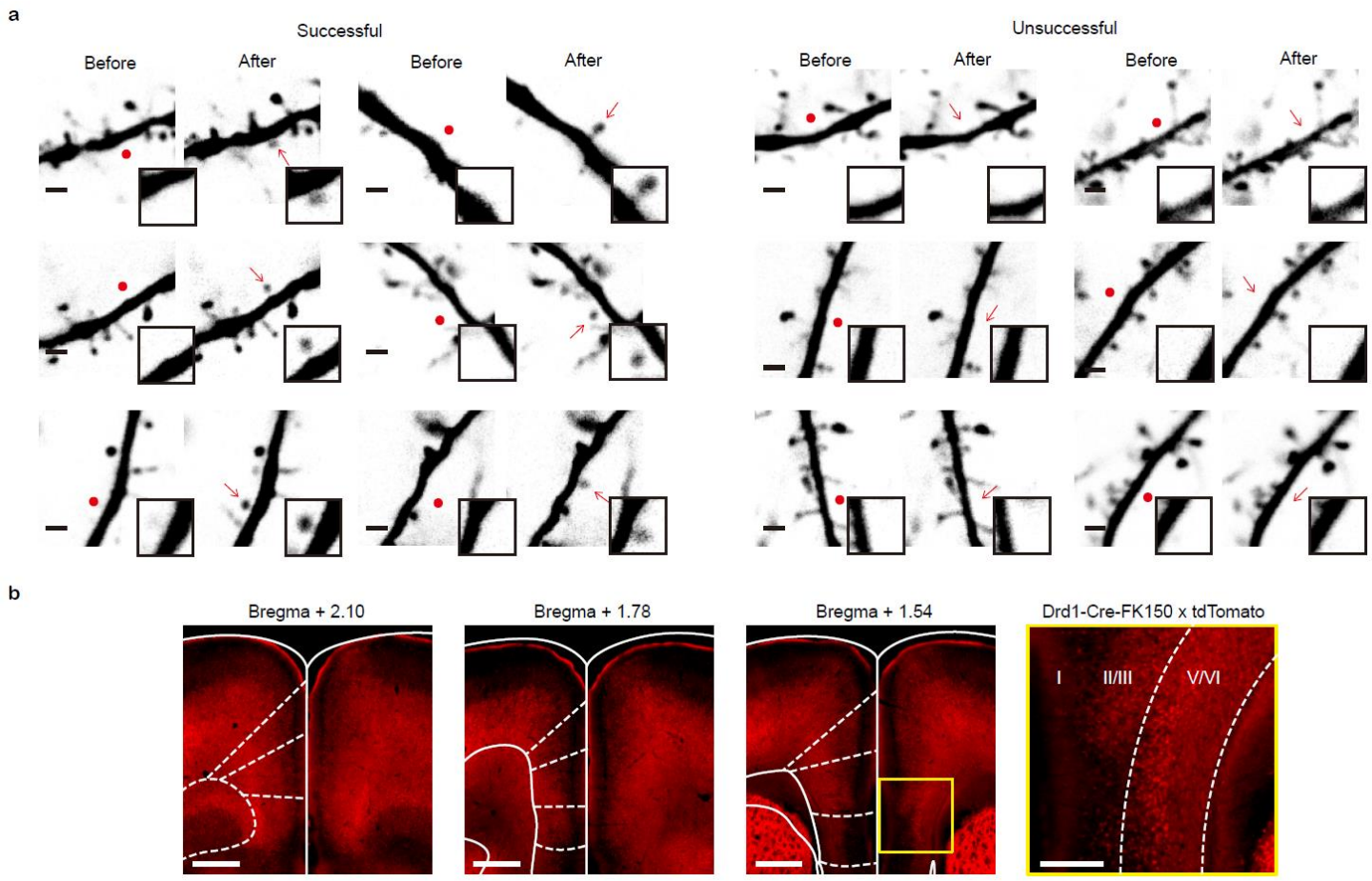

Extended Data Figure 4. ***De novo*** **glutamate-induced spinogenesis on pyramidal neurons in mPFC**

(a). Example 2PLSM images of successful and unsuccessful induction trials of *de novo* spinogenesis. Red circles, uncaging sites. Black rectangle, close up images of local dendritic segments before and after glutamate uncaging. Scale bar, 2 µm.

(b). Distribution of tdTomato^{+} neurons in mPFC in a Drd1-Cre-FK150; tdTomato reporter mouse. Close up image of mPFC shows the distribution of tdTomato^{+} neurons across cortical layers. Scale bars, 500 µm, 200 µm.

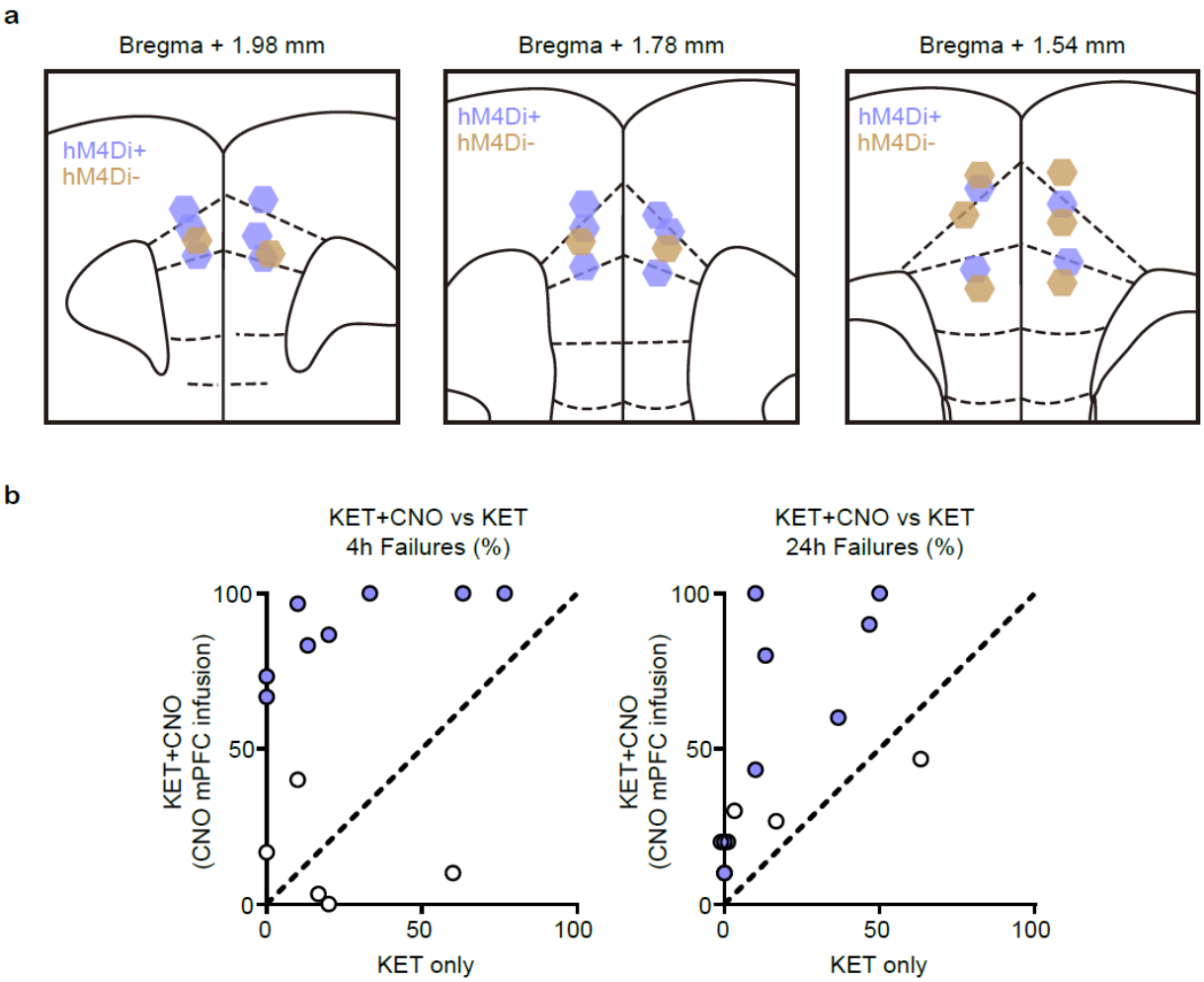

Extended Data Figure 5. Local inhibition of DA terminals in mPFC blocks the behavioral effect of ketamine

(a). Atlas locations showing cannula placements for data in Figure 6.

(b). Within subject summary data for behavioral responses (Figure 6C) after ketamine treatment, compared with ketamine + CNO (mPFC), 4 hrs and 24 hrs after treatment.

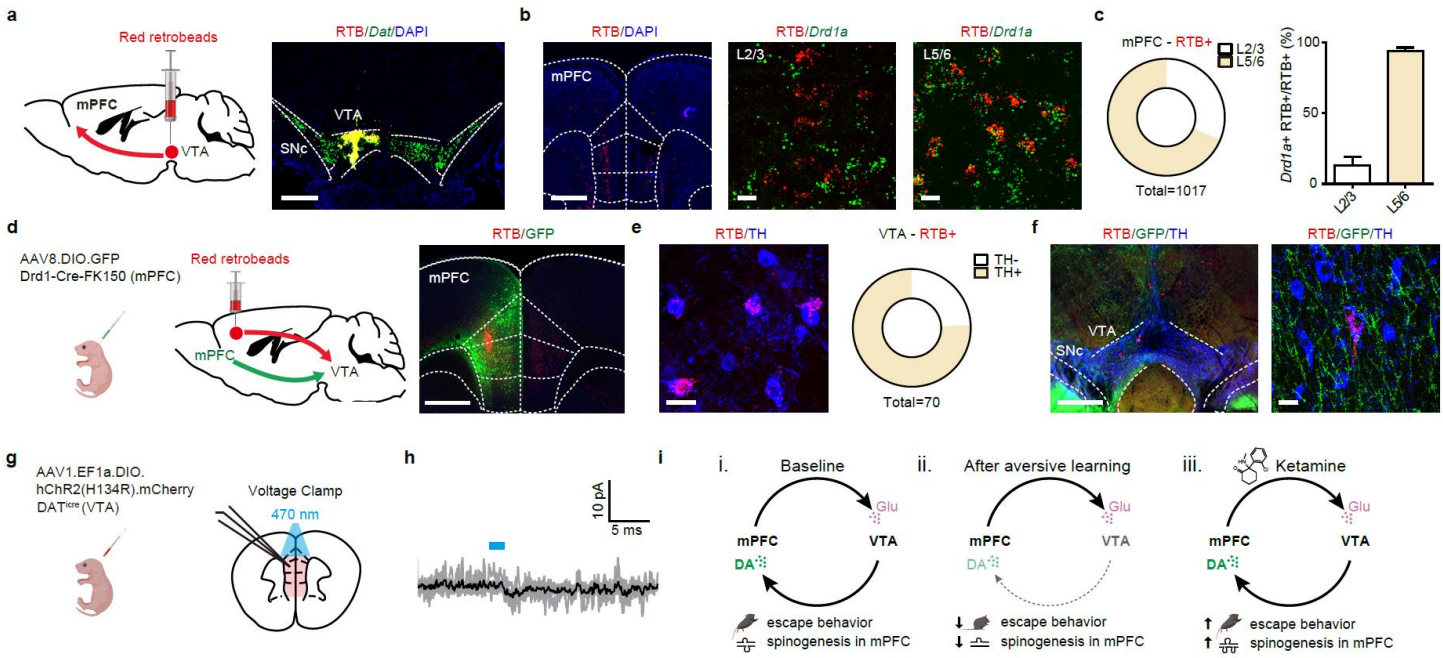

Extended Data Figure 6. Recurrent loops link DA-sensing mPFC and VTA DA neurons

(a). Left, schematic illustrating retrograde labeling strategy. Right, coronal image of retrobead (RTB) injection site. Red, retrobeads; green, *Da*t mRNA; blue, DAPI. Scale bar, 500 µm.

(b). Left, retrobead fluorescence in mPFC (atlas overlay, dashed line). Middle and right, colocalization of RTB and *Drd1* mRNA in superficial and deep layers of mPFC. Scale bars, 500 µm (left), 20 µm (middle and right).

(c). Left, the proportional distribution of RTB^+ neurons across superficial and deep cortical layers. Right, quantification of the percentage of *Drd1a*$^+$ cells among RTB^+ cells across layers. n = 2 animals, 31.3% RTB^+ neurons in layer 2/3, 68.7% RTB^+ in layer 5/6. Among those RTB^+ neurons, 13.2 ± 6.2% are *Drd1*$^+$ in layer 2/3, 94.1 ± 2.5 are *Drd1*$^+$ in layer 5/6.

(d). Left, schematic illustrating retrograde labeling with viral transduction strategy. Right, a coronal image showing RTB signal (red) and the expression of EGFP (green) in the mPFC. Scale bar, 500 µm.

(e). Left, example image showing the colocalization of RTB (red) and TH (blue) in the VTA. Right, the proportional distribution of TH^+ neurons among RTB^+ cells in the VTA. Scale bar, 20 µm. n = 4 animals, 75.7% TH^+.

(f). Left, example image of $EGFP^+$ terminals in the VTA and SNc (red, RTB; green, EGFP; blue, TH). Right, a close up image illustrating $EGFP^+$ terminals surrounding TH^+/RTB^+ neurons. Scale bars, 500 µm, 20 µm.

(g). Left, schematic illustrating viral transduction strategy. Right, schematic for voltage-clamp recordings of mPFC pyramidal neurons.

(h). Summary data for voltage-clamp recordings of mPFC pyramidal neurons with optogenetic stimulation of VTA DA terminals (470 nm, 2 ms, ~2 mW). Grey traces, optically evoked currents from individual neurons; black, average across cells. n = 5 cells from 2 animals.

(i). Schematic summary illustrating recurrent mPFC VTA circuits across learning states, with the observed effects on VTA DA activity, behavior, and mPFC plasticity.

References

1. Daly, E. J. *et al.* Efficacy and safety of intranasal esketamine adjunctive to oral antidepressant therapy in treatment-resistant depression: A randomized clinical trial. *JAMA Psychiatry* **75,** 139–148 (2018).

2. Berman, R. M. *et al.* Antidepressant effects of ketamine in depressed patients. *Biol. Psychiatry* **47,** 351–354 (2000).

3. Harmer, C. J., Duman, R. S. & Cowen, P. J. How do antidepressants work? New perspectives for refining future treatment approaches. *The Lancet Psychiatry* **4,** 409–418 (2017).

4. Fuchikami, M. *et al.* Optogenetic stimulation of infralimbic PFC reproduces ketamine's rapid and sustained antidepressant actions. *Proc. Natl. Acad. Sci.* **112,** 8106–8111 (2015).

5. Duman, R. S., & Aghajanian, G. K. Synaptic dysfunction in depression: potential therapeutic targets. *Science*, **338**(6103), 68-72 (2012).

6. Duman, R. S., Aghajanian, G. K., Sanacora, G. & Krystal, J. H. Synaptic plasticity and depression: New insights from stress and rapid-acting antidepressants. *Nat. Med.* **22,** 238–249 (2016).

7. Krishnan, V. & Nestler, E. J. Animal models of depression: molecular perspectives. *Curr. Top. Behav. Neurosci.* **7,** 121–47 (2011).

8. Li, N., et al. mTOR-dependent synapse formation underlies the rapid antidepressant effects of NMDA antagonists. *Science* **329**(5994), 959-964 (2010).

9. Popoli, M., Yan, Z., McEwen, B. S. & Sanacora, G. The stressed synapse: The impact of stress and glucocorticoids on glutamate transmission. *Nat. Rev. Neurosci.* **13,** 22–37 (2012).

10. Miller, O. H. *et al.* GluN2B-containing NMDA receptors regulate depression-like behavior and are critical for the rapid antidepressant actions of ketamine. *Elife* **3,** e03581 (2014).

11. Gerhard, D. M., Wohleb, E. S. & Duman, R. S. Emerging treatment mechanisms for depression: focus on glutamate and synaptic plasticity. *Drug Discov. Today* **21,** 454–464 (2016).

12. Moda-Sava, R. N. *et al.* Sustained rescue of prefrontal circuit dysfunction by antidepressant-induced spine formation. *Science* **364,** eaat8078 (2019).

13. Proulx, C. D., Hikosaka, O. & Malinow, R. Reward processing by the lateral habenula in normal and depressive behaviors. *Nat. Neurosci.* **17,** 1146–1152 (2014).

14. Abler, B., Erk, S., Herwig, U. & Walter, H. Anticipation of aversive stimuli activates extended amygdala in unipolar depression. *J. Psychiatr. Res.* **41,** 511–522 (2007).

15. Heldt, S. A., Stanek, L., Chhatwal, J. P. & Ressler, K. J. Hippocampus-specific deletion of BDNF in adult mice impairs spatial memory and extinction of aversive memories. *Mol. Psychiatry* **12,** 656–670 (2007).

16. Maier, S. F. & Seligman, M. E. Learned helplessness: Theory and evidence. *J. Exp. Psychol. Gen.* **105,** 3–46 (1976).

17. LY, A., MEP, S. & JD, T. Learned helplessness in humans: critique and reformulation. *J. Abnorm. Psychol.* **87,** 49 (1978).

18. Seligman, M. E. & Maier, S. F. Failure to escape traumatic shock. *J. Exp. Psychol.* **74,** 1–9 (1967).

19. Maier, S. F. & Seligman, M. E. P. Learned helplessness at fifty: Insights from neuroscience. *Psychol. Rev.* **123,** 1–19 (2016).

20. Morales, M. & Margolis, E. B. Ventral tegmental area: Cellular heterogeneity, connectivity and

behaviour. *Nat. Rev. Neurosci.* **18,** 73–85 (2017).

21. Lammel, S., Lim, B. K. & Malenka, R. C. Reward and aversion in a heterogeneous midbrain dopamine system. *Neuropharmacology* **76,** 351–359 (2014).

22. Tsai, H.-C. *et al.* Phasic firing in dopaminergic neurons is sufficient for behavioral conditioning. *Science* **324**(5930), 1080–1084 (2009).

23. Tan, K. R. *et al.* GABA neurons of the VTA drive conditioned place aversion. *Neuron* **73,** 1173–1183 (2012).

24. Watabe-Uchida, M., Eshel, N. & Uchida, N. Neural circuitry of reward prediction error. *Annu. Rev. Neurosci.* **40,** 373–394 (2017).

25. Hollon, N. G., Burgeno, L. M. & Phillips, P. E. M. Stress effects on the neural substrates of motivated behavior. *Nat. Neurosci.* **18,** 1405–1412 (2015).

26. Russo, S. J. & Nestler, E. J. The brain reward circuitry in mood disorders. *Nat. Rev. Neurosci.* **14,** 609–625 (2013).

27. Grace, A. A. Dysregulation of the dopamine system in the pathophysiology of schizophrenia and depression. *Nature Reviews Neuroscience* **17,** 524–532 (2016).

28. Chaudhury, D. *et al.* Rapid regulation of depression-related behaviours by control of midbrain dopamine neurons. *Nature* **493,** 532–536 (2013).

29. Friedman, A. K. *et al.* Enhancing depression mechanisms in midbrain dopamine neurons achieves homeostatic resilience. *Science* **344**(6181), 313–9 (2014).

30. Tye, K. M. *et al.* Dopamine neurons modulate neural encoding and expression of depression-related behaviour. *Nature* **493,** 537–541 (2012).

31. Kokkinou, M., Ashok, A. H. & Howes, O. D. The effects of ketamine on dopaminergic function: Meta-Analysis and review of the implications for neuropsychiatric disorders. *Mol. Psychiatry* **23,** 59–69 (2018).

32. Belujon, P. & Grace, A. A. Restoring mood balance in depression: Ketamine reverses deficit in dopamine-dependent synaptic plasticity. *Biol. Psychiatry* **76,** 927–936 (2014).

33. Chourbaji, S. *et al.* Learned helplessness: Validity and reliability of depressive-like states in mice. *Brain Res. Protoc.* **16,** 70–78 (2005).

34. de Jong, J. W. *et al.* A neural circuit mechanism for encoding aversive stimuli in the mesolimbic dopamine system. *Neuron* **101,** 133–151.e7 (2019).

35. Howe, M. W. & Dombeck, D. A. Rapid signalling in distinct dopaminergic axons during locomotion and reward. *Nature* **535,** 505–510 (2016).

36. da Silva, J. A., Tecuapetla, F., Paixão, V. & Costa, R. M. Dopamine neuron activity before action initiation gates and invigorates future movements. *Nature* **554,** 244–248 (2018).

37. Honey, G. D. *et al.* Individual differences in psychotic effects of ketamine are predicted by brain function measured under placebo. *J. Neurosci.* **28,** 6295–303 (2008).

38. Roth, B. L. DREADDs for neuroscientists. *Neuron* **89,** 683–94 (2016).

39. Armbruster, B. N., Li, X., Pausch, M. H., Herlitze, S. & Roth, B. L. Evolving the lock to fit the key to create a family of G protein-coupled receptors potently activated by an inert ligand. *Proc. Natl. Acad. Sci.* **104,** 5163–5168 (2007).

40. Kozorovitskiy, Y., Saunders, A., Johnson, C. A., Lowell, B. B. & Sabatini, B. L. Recurrent network

activity drives striatal synaptogenesis. *Nature* **485,** 646–650 (2012).

41. Kozorovitskiy, Y., Peixoto, R., Wang, W., Saunders, A. & Sabatini, B. L. Neuromodulation of excitatory synaptogenesis in striatal development. *Elife* **4**, e10111 (2015).

42. Yang, H. *et al.* Nucleus accumbens subnuclei regulate motivated behavior via direct Inhibition and disinhibition of VTA dopamine subpopulations. *Neuron* **97,** 434–449.e4 (2018).

43. Wass, C., Sauce, B., Pizzo, A. & Matzel, L. D. Dopamine D1 receptor density in the mPFC responds to cognitive demands and receptor turnover contributes to general cognitive ability in mice. *Sci. Rep.* **8,** 4533 (2018).

44. Ferenczi, E. A. *et al.* Prefrontal cortical regulation of brainwide circuit dynamics and reward-related behavior. *Science* **351**(6268), aac9698 (2016).

45. Vander Weele, C. M. *et al.* Dopamine enhances signal-to-noise ratio in cortical-brainstem encoding of aversive stimuli. *Nature* **563,** 397–401 (2018).

46. Patriarchi, T. *et al.* Ultrafast neuronal imaging of dopamine dynamics with designed genetically encoded sensors. *Science* **360**(6396), eaat4422 (2018).

47. Okubo, Y. *et al.* Decreased prefrontal dopamine D1 receptors in schizophrenia revealed by PET. *Nature* **385,** 634–636 (1997).

48. Dong, Y., White, F. J., Lavin, A. & Seamans, J. K. Dopamine D1-class receptors selectively modulate a slowly inactivating potassium current in rat medial prefrontal cortex pyramidal neurons. *J. Neurosci.* **23,** 2686–95 (2003).

49. Floresco, S. B., Magyar, O., Ghods-Sharifi, S., Vexelman, C. & Tse, M. T. L. Multiple dopamine receptor subtypes in the medial prefrontal cortex of the rat regulate set-shifting. *Neuropsychopharmacology* **31,** 297–309 (2006).

50. Duman, R. S., Li, N., Liu, R.-J., Duric, V. & Aghajanian, G. Signaling pathways underlying the rapid antidepressant actions of ketamine. *Neuropharmacology* **62,** 35–41 (2012).

51. Phoumthipphavong, V., Barthas, F., Hassett, S. & Kwan, A. C. Longitudinal effects of ketamine on dendritic architecture in vivo in the mouse medial frontal cortex. *eNeuro* **3**(2), (2016).

52. Sarkar, A. & Kabbaj, M. Sex differences in effects of ketamine on behavior, spine density, and synaptic proteins in socially isolated rats. *Biol. Psychiatry* **80,** 448–456 (2016).

53. Ng, L. H. L. *et al.* Ketamine and selective activation of parvalbumin interneurons inhibit stress-induced dendritic spine elimination. *Transl. Psychiatry* **8,** 272 (2018).

54. Kwon, H.-B. & Sabatini, B. L. Glutamate induces de novo growth of functional spines in developing cortex. *Nature* **474,** 100–104 (2011).

55. Guo, L. *et al.* Dynamic rewiring of neural circuits in the motor cortex in mouse models of Parkinson's disease. *Nat. Neurosci.* **18,** 1299–1309 (2015).

56. Tritsch, N. X. & Sabatini, B. L. Dopaminergic modulation of synaptic transmission in cortex and striatum. *Neuron* **76,** 33–50 (2012).

57. Stachniak, T. J., Ghosh, A. & Sternson, S. M. Chemogenetic synaptic silencing of neural circuits localizes a hypothalamus→midbrain pathway for feeding behavior. *Neuron* **82,** 797–808 (2014).

58. Mahler, S. V *et al.* Designer receptors show role for ventral pallidum input to ventral tegmental area in cocaine seeking. *Nat. Neurosci.* **17,** 577–585 (2014).

59. Shen, W., Flajolet, M., Greengard, P. & Surmeier, D. J. Dichotomous dopaminergic control of striatal

synaptic plasticity. *Science* **321**(5890), 848–851 (2008).

60. Hare, B. D. *et al.* Optogenetic stimulation of medial prefrontal cortex Drd1 neurons produces rapid and long-lasting antidepressant effects. *Nat. Commun.* **10,** 223 (2019).

61. Lodge, D. J. The medial prefrontal and orbitofrontal cortices differentially regulate dopamine system function. *Neuropsychopharmacology* **36,** 1227–36 (2011).

62. Xiao, L., Priest, M. F. & Kozorovitskiy, Y. Oxytocin functions as a spatiotemporal filter for excitatory synaptic inputs to VTA dopamine neurons. *Elife* 7 e33892 (2018).

63. Beier, K. T. *et al.* Circuit architecture of VTA dopamine neurons revealed by systematic input-output mapping. *Cell* **162,** 622–634 (2015).

64. Tecuapetla, F. *et al.* Glutamatergic signaling by mesolimbic dopamine neurons in the nucleus accumbens. *J. Neurosci.* **30,** 7105–7110 (2010).

65. Maier, S. F. Learned helplessness and animal models of depression. *Prog. Neuropsychopharmacol. Biol. Psychiatry* **8,** 435–46 (1984).

66. Berridge, K. C. & Kringelbach, M. L. Pleasure systems in the brain. *Neuron* **86,** 646–664 (2015).

67. Schultz, W. Dopamine reward prediction-error signalling: a two-component response. *Nat. Rev. Neurosci.* **17,** 183–195 (2016).

68. Nestler, E. J. & Carlezon, W. A. The mesolimbic dopamine reward circuit in depression. *Biol. Psychiatry* **59,** 1151–1159 (2006).

69. Morris, G., Nevet, A., Arkadir, D., Vaadia, E. & Bergman, H. Midbrain dopamine neurons encode decisions for future action. *Nat. Neurosci.* **9,** 1057–1063 (2006).

70. Enomoto, K. *et al.* Dopamine neurons learn to encode the long-term value of multiple future rewards. *Proc. Natl. Acad. Sci. U. S. A.* **108,** 15462–7 (2011).

71. Bromberg-Martin, E. S. & Hikosaka, O. Midbrain dopamine neurons signal preference for advance information about upcoming rewards. *Neuron* **63,** 119–126 (2009).

72. Holmes, S. E. *et al.* Lower synaptic density is associated with depression severity and network alterations. *Nat. Commun.* **10,** 1529 (2019).

73. Bäckman, C. M. *et al.* Characterization of a mouse strain expressing Cre recombinase from the 3′ untranslated region of the dopamine transporter locus. *Genesis* **44,** 383–390 (2006).

74. Gong, S. *et al.* Targeting Cre recombinase to specific neuron populations with bacterial artificial chromosome constructs. *J. Neurosci.* **27,** 9817–23 (2007).

75. Chen, T.-W. *et al.* Ultrasensitive fluorescent proteins for imaging neuronal activity. *Nature* **499,** 295–300 (2013).

76. Krashes, M. J. *et al.* Rapid, reversible activation of AgRP neurons drives feeding behavior in mice. *J. Clin. Invest.* **121,** 1424–1428 (2011).

77. Hou, X. H. *et al.* Central control circuit for context-dependent micturition. *Cell* **167,** 73–86.e12 (2016).

78. Pologruto, T. A., Sabatini, B. L. & Svoboda, K. ScanImage: Flexible software for operating laser scanning microscopes. *Biomed. Eng. Online* **2,** 13 (2003).

79. Xiao, L., Priest, M. F., Nasenbeny, J., Lu, T. & Kozorovitskiy, Y. Biased oxytocinergic modulation of midbrain dopamine systems. *Neuron* **95,** 368–384.e5 (2017).

80. Coupé, P., Munz, M., Manjón, J. V., Ruthazer, E. S., & Collins, D. L. A CANDLE for a deeper in vivo

insight. *Medical Image Analysis* **16**(4), 849-864 (2012).

81. Schindelin, J. *et al.* Fiji: an open-source platform for biological-image analysis. *Nat. Methods* **9,** 676–82 (2012).

82. Rodriguez, A. *et al. ToxTrac* : A fast and robust software for tracking organisms. *Methods Ecol. Evol.* **9,** 460–464 (2018).